2006

The Role of Sulfatide in Alzheimer's Disease

Charles Britton Beasley Jr.
Virginia Commonwealth University

`THE ROLE OF SULFATIDE IN ALZHEIMER'S DISEASE

A thesis submitted in partial fulfillment of the requirements for the degree of Master's in Anatomy and Neurobiology at Virginia Commonwealth University.

by

CHARLES BRITTON BEASLEY, JR.
B.S. Biology

Director: JEFFREY DUPREE, PHD
ASSISTANT PROFESSOR, DEPARTMENT OF ANATOMY AND NEUROBIOLOGY

Virginia Commonwealth University
Richmond, Virginia
August, 2006

Table of Contents

List of Tables

Page

List of Figures

Page

List of Abbreviations

Aβ	Amyloid Beta
AD	Alzheimer's Disease
ANOVA	Analysis of variance
APP	Amyloid precursor protein
C	Cerebroside
CASPR	CASPR/Paranodin/NCP1
Ch	Cholesterol
CNP	2',3'-Cyclic nucleotide 3'-phosphodiesterase
CNS	Central nervous system
CST	Cerebroside sulfotransferase
GalC	Galactocerebroside
GM	Gray matter
IHC	Immunohistochemistry
KO	Knockout
LF	Lipofuscin
MT	Microtubule
NaCh	Sodium channel
Nfasc	Neurofascin
NFT	Neurofibrillary tangle
OCT	Optimum Cutting Temperature
OL	Oligodendrocyte
PBS	Phosphate buffered saline
PHF	Paired helical filaments
PNS	Peripheral nervous system
SD	Standard deviation
ST	Sulfatide
TLC	Thin layer chromatography
UCLA	University of California at Los Angeles brain bank
WM	White matter

Abstract

THE ROLE OF SULFATIDE IN ALZHEIMER'S DISEASE

By Charles Britton Beasley, Jr., B.S. Biology

A Thesis submitted in partial fulfillment of the requirements for the degree of Master's in Anatomy and Neurobiology at Virginia Commonwealth University.

Virginia Commonwealth University, 2006

Major Director: Jeffrey Dupree, Ph.D.
Assistant Professor, Department of Anatomy and Neurobiology

Alzheimer's disease (AD) is characterized by the accumulation of amyloid beta plaques, neurofibrillary tangles (NFT) and loss of cortical neurons that control memory and cognition. The cause of NFTs and Aβ plaques is not clear, though it is known that they are formed by enzymes which are preferentially sequestered to membrane domains called lipid rafts. Sulfatide (ST) is a glycosphingolipid that is essential for the proper structure and function of lipid rafts. In mice that lack ST, membrane domains that are normally maintained by adhesive contacts and functional lipid rafts are improperly formed and are unstable. In these ST null mice, voltage gated sodium channels, neuronal proteins that

normally cluster at the nodes of Ranvier, initially accumulate in the node but are not retained with age. Taken together the findings from the ST null mice indicate that membrane organization is compromised. Recently, a published report demonstrated that ST is significantly reduced in AD. Based on this observation combined with the findings from the ST null mice, I propose that membrane architecture is also altered in AD and this alteration may facilitate AD pathogenesis. To test this hypothesis, I have used an immunohistochemical approach to assess neuronal membrane organization in AD and non-AD brain samples. Analysis of the sodium channel clusters was chosen since these nodal domains provide an easy assessment tool for membrane organization. In the current study, sodium channel domains were not altered and no change in isoform expression was observed. Based on these findings, membrane organization does not appear to be altered in AD. It is important to note, however, that sodium channel clusters are restricted to a specific region of the axon and thus membrane organization within other regions of the axon and in other regions of the neuron may be altered. Additionally, assessment of the brain samples, using thin layer chromatography, did not show a reduction in ST levels between the AD and non-AD brains. Therefore, my study strongly suggests that further analysis of ST levels in AD brains sould be conducted to resolve the contrasting results between the current study and the previously published work.

Introduction

Overview of Alzheimer's Disease

Alzheimer's disease (AD) is the most prevalent cause of neural degeneration and dementia in the rapidly growing elderly population. Patients with AD experience mild to severe dementia including progressive memory loss. Though the trends resemble those of the normal aging brain, symptoms are significantly exaggerated in AD. Age is the most important risk factor. The characteristic pathologies at the microscopic level are amyloid beta (Aβ) plaques and neurofibrillary tangles (NFT). Though these are well-established indicators, much remains to be understood about their formation. (reviewed by Armstrong, 2006).

Diagnosis of AD involves both psychological analysis for the presence and level of dementia and post-mortem morphological testing for Aβ plaques and NFTs. The mini-mental state examination (MMSE) and the AD assessment scale (ADAS) are both used as objective measures of progression of cognitive impairment (Schmitt et al., 2002). In addition to the MMSE and ADAS classifications, Braak and Braak (1991) developed a staging system for the disease that is based on the degree and location of NFTs. Braak and Braak demonstrated that levels of AD correlated with the patterns and extent of NFT formation. In this system, stages I and II are characterized by mild to severe alteration of

the transentorhinal layer; stages III and IV involve the proper entorhinal cortex, and stages V and VI show destruction of isocortical association areas as well. Magnetic resonance imaging for loss of gray and white matter is also used in the diagnosis (Karas et al., 2004; Sjobeck et al., 2006).

AD can be divided into familial and non-familial categories. Familial AD is usually associated with early onset and often involves mutations in the APP gene or presenilins. Gottries et al., (1996) used confusional symptomatology and parietal pathology to differentiate between the two categories. Parietal pathology was associated more with the early AD and confusioanl symptomatology with late onset.

The cause of Alzheimer's remains unknown. Various treatments including acetylchoinesterase (AChE) inhibitors and new experimental therapies using Aβ antibodies have been used with minimal success. AChE has been very effective in providing incremental increase in cognitive ability by increasing levels of acetylcholine, but has no effect on the underlying pathology. The use of antibodies is still under examination.

Histopathology of Alzheimer's Disease

The underlying cause of dementia in AD is loss of neurons. Specifically, this loss is seen in pyramidal and interneurons in the entorhinal neocortices, the nucleus basalis, basal forebrain, and pyramidal neurons in the CA1 and CA2 regions of the hippocampus. This loss of cells leads to gross brain changes such as reduction in overall brain size, widened sulci, narrowed gyri, and dilated ventricles. Microscopic analysis using silver

stains reveals the two hallmark pathologies that are NFTs and Aβ plaques (Figure 1). NFTs are found intracellularly and Aβ plaques extracellularly (DeArmond, 1997).

NFTs are not unique to AD, although they are a necessary histological finding for AD diagnosis (Braak and Braak, 1991). They are also found in Parkinson's and amyotrophic lateral sclerosis (Kokubo and Kuzuhara, 2004). Tangles are formed in neuronal cell bodies as a result of hyperphosphorylation of the microtubule associated protein tau. Hyperphosphorylation of tau results in the formation of paired helical filaments (PHF), which are the building blocks of NFTs. Microtubule associated protein kinase, glycogen synthase kinase-3, cyclin-dependant kinase 2, cyclin-dependant kinase 5, calcium/calmodulin-dependent protein kinase II, protein kinase A, and fyn kinase have been shown to be involved in this hyperactive phosphorylation (Drewes et al., 1992; Madelkow et al., 1992; Baumann et al., 1993). Fyn and cdk are associated with lipid rafts as well (Kramer et al., 1999). Reduced phosphatase activity has also been reported in AD and implicated in the formation of tangles (Matsuo et al., 1994; Iqbal et al., 1994). Though tau is normally phosphorylated only at sites outside the microtubule (MT) binding region, in PHFs phosphorylation is found at sites within the MT binding region (De Armond, 1997).When abnormally phosphorylated, tau does not bind properly to MTs, but rather associates with itself (De Armond, 1997).

Figure 1: Hallmark histopathologies in Alzheimer's disease: neurofibrillary tangles and amyloid beta plaques. (Taken from American Health Assistance Foundation: http://www.ahaf.org/alzdis/about/AmyloidPlaques.htm)

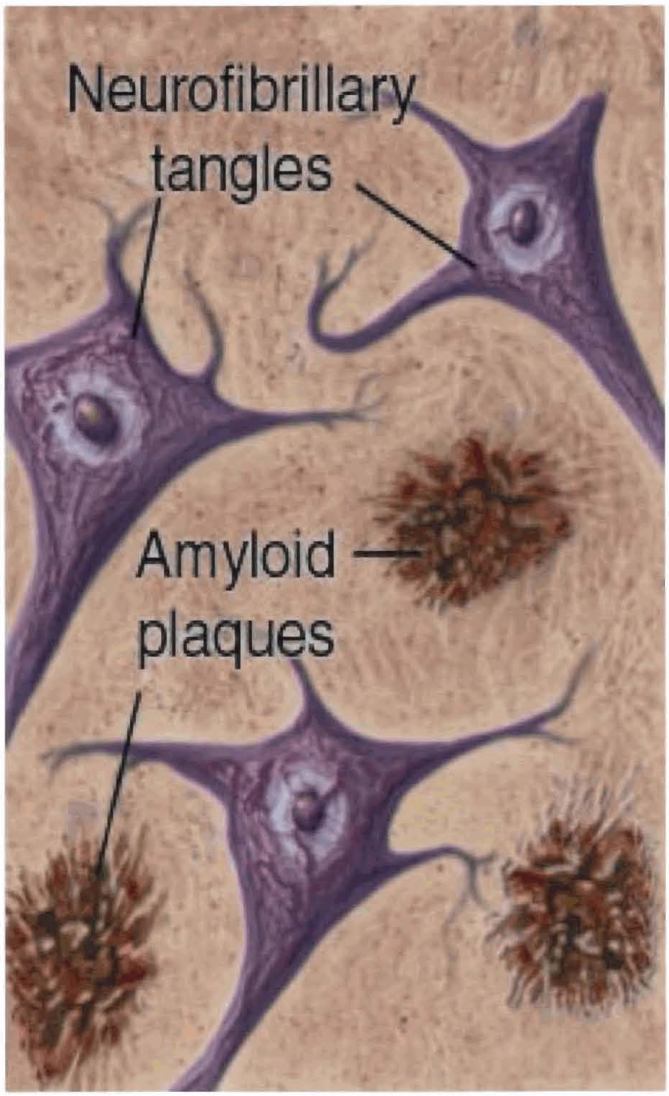

Figure 1: Illustration of neurofibrillary tangles and amyloid beta plaques

The theoretical course then, by which NFTs prove toxic to neurons consists of the following steps as described by Trojanowski and Lee, (2005): First, the abnormal hyperphosphorylation of tau leads to tau aggreagation. This leads to a decrease in MT-bound tau and then to MT depolymerization. Axonal transport is impaired as a result, and leads to stasis and aggregation of axonal traffic. Function at the synapse is compromised and axons degenerate and disconnect.

As mentioned above, Aβ plaques are the other of the classic neuropathologic hallmarks of AD and are also required for AD diagnosis. These plaques are the product of an alternate cleavage of the type I transmembrane protein, amyloid precursor protein (APP) (Figure 2). APP is ubiquitously expressed protein whose function remains unclear. There are two types of APP cleavage, alpha-gamma and beta-gamma, both of which occur on the lumenal side of membranes (Greenfield et al., 1999). The alpha-gamma cleavage (non-amyloidogenic) consists of a cut at the alpha site by alpha-secretases, which occurs at the cell membrane. Several zinc metaloproteinases and the aspartyl proteinase beta-amyloid cleavage enzyme 2, that are present mostly at the cell surface, are responsible for the cut at the alpha site. This cleavage is followed by another cut at the gamma site within the transmembrane domain of APP by the multimeric protein complex known as the gamma secretase. The gamma cleavage occurs mainly in endocytotic vesicles The alpha-gamma sequence is the normal non-pathologic event that occurs 95% of the time.

In AD, the beta-gamma (amyloidogenic) sequence becomes more prevalent, resulting in the deposit of the toxic Aβ peptides (Vetrivel and Thinakaran, 2006). In this

pathologic state, the alpha cleavage is replaced by a beta-cleavage occuring mainly on the membrane of endocytotic vesicles by the membrane bound beta-amyloid cleavage enzyme 1 (BACE 1 or just BACE). Aβ peptides are exocytosed and accumulate to form plaques or soluble oligomers in the extracellular space. This accumulation primarily occurs in the cerebral cortex in associational areas (Hof and Mobbs, 2001) and is considered to be one of the early events of AD. Although the direct consequence of these Aβ aggregates is unknown, they may contribute to inflammation (reviewed by Minghettis, 2005) and altered ion transport (as reviewed by Kourie, 2001), both of which are possible players in AD.

Aβ peptides are found in several isoforms including 1-40, 1-42, and 1-43 called protofibrils (Figure 2). The 42 residue protofibril has the highest tendency to aggregate and accumulate in the extracellular space. Although the 1-40 isoform does aggreagate, these oligomers are very unstable. The amyloid cascade hypothesis, which has been one of the most prominent theories of AD pathogenesis, holds that the fibrillar plaques formed by Aβ 1-42 are responsible for neuronal death (reviewed by Klein, 2002). Evidence has shown that the location of insoluble Aβ shows poor correlation to the region of cell death, and quantity of these plaques show poor association with degree of dementia (reviewed by Klein, 2002). Soluble oligomers of Aβ 1-42 however have a significant correlation with synapse loss. Levels of 1-42 are correlated with memory loss and regionally associated with neuron death, making soluble Aβ seem the more likely culprit in Aβ.

Figure 2: a) Location and amino acid sequence of amyloid precursor protein. β and α cleavage sites shown on the luminal side of the membrane. γ cleavage sites (40 and 42) shown in the intramembrane domain. b) Non-amyloidogenic sequence of cleavage events (α followed by γ). c) Amyloidogenic (pathologic) cleavage sequence (β followed by γ). (taken from Vetrivel and Thinakaran, 2006)

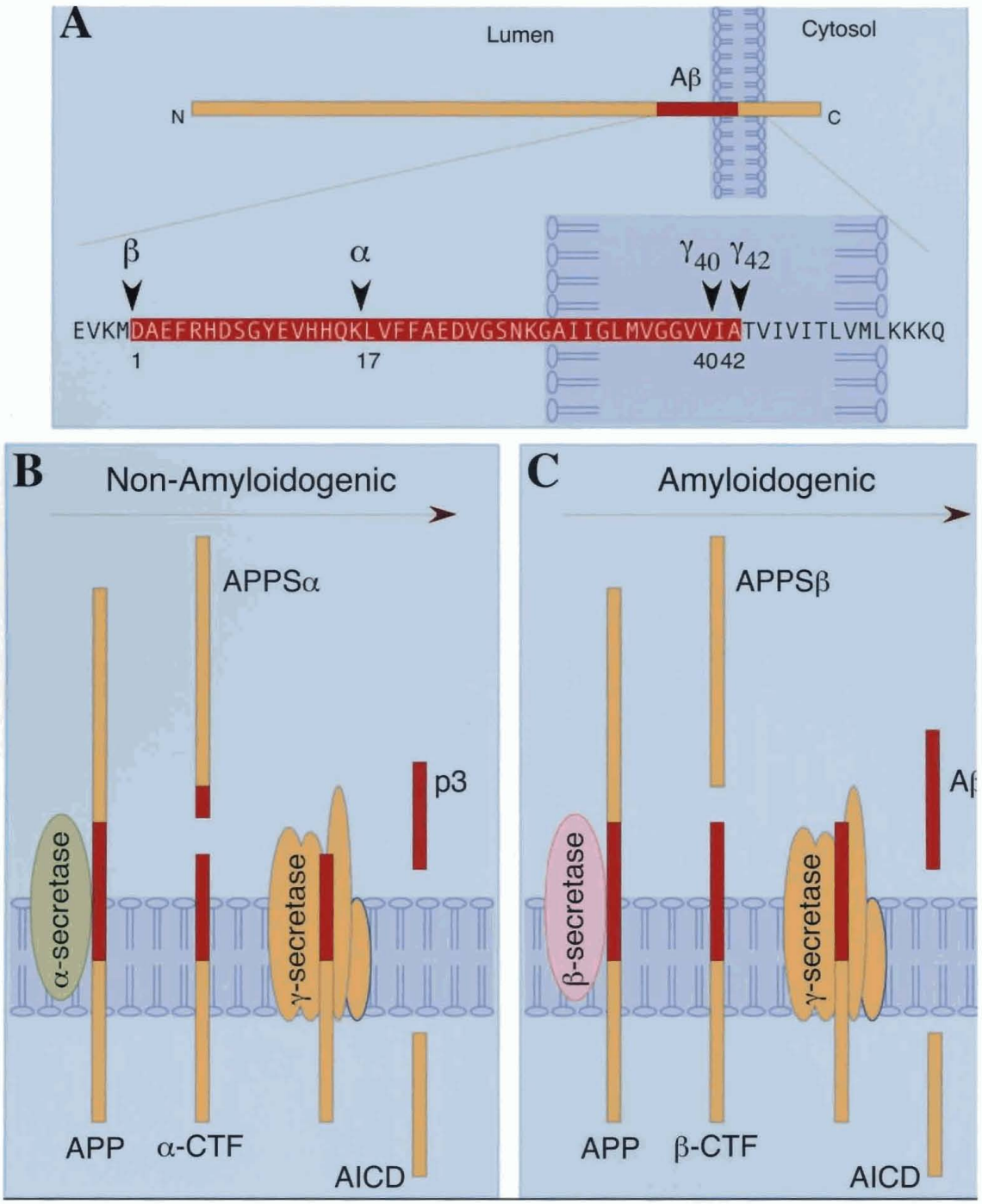

Figure 2: Structure and cleavage of amyloid precursor protein

The means by which NFTs and Aβ form are unknown for non-familial AD. One possibility for the pathogensis is that the enzymes that generate these pathologies become abnormally localized in membrane domains called lipid rafts.

Lipid Rafts and Sphingolipids

The traditional model of cell membrane architecture describes a homogenous free-floating lateral organization of the cell membrane, though it has become clear that domains of tight lipid packing occur especially in the outer leaflet. These domains are highly enriched in cholesterol and sphingolipids that are able to pack tightly due to weak interactions of the carbohydrate head groups of the glycosphingolipids (as reviewed by Simons and Ikonen, 1997) and saturation of their hydrocarbon chains. These rafts are able to move freely within the membrane and can cluster upon interaction of the proteins that are associated with them (as reviewed by Rajendran and Simons, 2005). Various proteins preferentially partition into the rafts such as glycosylphosphatidyl-inositol (GPI)-anchored proteins, tyrosine kinases, G-proteins and other transmembrane proteins (Rajendron and Simons, 2004). These proteins are likely recruited to these membrane microdomains for the purpose of signaling and adhesion. Some of these proteins include enzymes whose activity is influenced by the integrity and clustering of these rafts (as reviewed by Simons and Ikonen, 1997).

Interestingly, it has been recently shown that one of these glycosphingolipids, Sulfatide (ST) has levels that are uniquely reduced in AD. Han et al. (2002) showed that ST is decreased in AD tissue using mass spectrometry, and Gottfries et al. (1996) obtained

the same results using thin layer chromatography. This loss of ST and ensuing disturbance of lipid rafts may lead to abnormal distribution of enzymatic activity in the brain, resulting in the formation of the hallmark histopathologies of AD.

It has been suggested that rafts may be involved in the formation of Aβ plaques and NFTs of AD via the improper recruitment of enzymes or loss of compartmentalization (as reviewed by Cordy et al., 2006). The secretases and kinases that form the plaques and tangles, respectively, are known to be preferentially partitioned into these membrane domains (Kramer et al., 1999). Abnormal proportions of raft lipids have been shown to alter the affinities of these enzymes for rafts and therefore enzymatic activity (Kalvodova et al., 2005; Kramer et al., 1999).

One example of enzyme activity conveyed by aggregation of raft proteins is that of fyn kinase as evidenced by Kramer et al. (1999). This example is especially relevant to the study at hand since fyn is involved in the hyper-phosphorylation of tau which results in NFTs (Lee et al., 2004). Glycoshpingolipids such as sulfatide, which are enriched in rafts, are synthesized at the same stage in the maturing OL as fyn coupled GPI-linked proteins get associated into rafts. In these early myelinating cells fyn kinase is highly active and linked to rafts. In OL progenitors or other membranes without rafts, fyn does not show the same activity. Also, addition of an antibody that leads to crosslinking of this fyn-coupled protein increases fyn activity. These results suggest that rafts are in fact a necessary platform for fyn enzyme activity that is directly implicated in formation of one of the hallmark AD microscopic pathologies (Kramer, 1999).

Cyclin dependant kinase 5 (cdk5) is also very pertinent to a raft-related theory of AD pathogenesis. Cdk5 is another of the numerous kinases responsible for the hyperphosphorylation of tau (Bauman et al., 1993). Furthermore, cdk5 activity is regulated by p35, and activator that associates with the cell membrane (Monaco et al., 2004), potentially with lipid rafts through N-terminal myristalation (Giese et al., 2005). Griffith et al. (2004) recently showed that only plasma membrane associated cdk5, which was complexed with p35, displayed activity. Improper membrane recruitment of this activator results in the mislocalized and prolonged activity of cdk5 potentially inducing tau hyperphosphorylation (Patrick et al., 1999)

APP is also associated with lipid rafts. It has also been shown that BACE, the enzyme responsible for the β-cleaveage of APP (Hussain et al., 1999), is selectively partitioned into rafts (Ehehalt et al., 2003). This occurs since BACE undergoes palmitoylation, which targets proteins to rafts (as reviewed by Vetrivel and Thinakaran, 2006). Addition of a GPI-anchor, which localizes proteins to rafts, to BACE increased the cleavage of APP at the β site (Cordy et al., 2003; Ehehalt et al., 2003). All four components of the gamma-secretase complex are also localized to these detergent insoluble membrane regions (Vetrivel et al., 2004). Also, Chen et al. (2006) showed that the intracellular domain of APP is associated with the raft protein flotillin-1. Using in vitro experiments in which concentrations of lipids found in rafts were varied, Kalvadova et al. (2005) showed that the ratio of lipids directly affects the activity of BACE. In addition, the alpha secretases responsible for normal processing of APP have not been linked to these lipid microdomains (Ehehalt et al., 2003).

A critical problem is how to test our hypothesis that altered raft formation due to reduced ST leads to AD pathogenesis. To possibly solve this dilemma, we will draw on results from our laboratory studying a knockout mouse in which the synthetic enzyme for Sulfatide, cerebroside sulfotransferase (CST), has been eliminated. ST is greatly enriched in oligodendrocytes (Norton et al., 1975), the myelin-forming cells in the CNS. Interestingly, the knockout animals consistently show dramatic changes in the myelin sheath, and specifically in the axonal-oligodendroglial junctions in the paranodal region, which is normally maintained by adhesion molecules sequestered into lipid rafts. Importantly, these mutant animals show altered distributions of ion channels which are normally uniquely sequestered in the axon plasma membrane. Since this re-distribution has been seen in the mutant animals due to loss of ST and potentially abnormal lipid rafts, we will examine AD brains for a similar redistribution which may be reflective of more global membrane changes specifically related to the pathogenesis of AD. Furthermore, the ST knockout mouse shows gray matter (GM) changes including neuronal death (Marcus et al., 2006), a finding consistent with AD pathology. The following sections briefly discuss the role of ST in nervous tissue, the importance of normal axon-oligodendroglial junctions and summarizes our results from experiements utilizing the CST mutant animals.

The role of ST in axon-oligodendroglial interactions

ST is a glycosphingolipid predominately synthesized by OLs in the CNS and therefore primarily found in myelin (Vos et al., 1994; Han et al., 2002). ST is found in hydroxylated and non-hydroxylated forms. The hydroxyl group is on the alpha carbon of

the fatty acid chain. Carbon chain lengths of ST vary from 16 to 26. ST is present in white matter (WM) and GM although it is much more prevalent in WM (Han et al., 2002; Krafft et al., 2005). ST accumulation due to enzymatic dysfunctions is involved in the pathogenesis of various human diseases such as metachromatic leukodystrophy and Krabbe's Disease (Han et al., 2002). Cerebroside sulfotransferase (CST) synthesizes ST by the sulfation of galactocerebroside (GalC) (Honke et al., 1997) (Figure 3). ST mediates various biological processes such as cell regulation, protein trafficking, signal transduction, cell adhesion, neuronal plasticity, and morphogenesis (reviews by Vos et al., 1994; Ishizuka, 1997; and Merrill et al., 1997).

ST may regulate neuronal viability by involvement in interactions between axons and OLs. Also, OLs are required for development, function and survival of neurons. The interaction of the axon and OL at the paranode is likely the means through which OLs are involved in these functions. One way ST may mediate axo-glial interactions is via the maintenance of OL membrane domains.

Axon-oligodendroglial junctions

The junction of the myelin sheath and the axon is characterized primarily by the interactions of several membrane proteins at the paranode that serve in adhesion (Menegoz et al., 1997), signaling (reviewed by Arroyo and Scherer, 2000), and membrane compartmentalization (Einheber et al., 1997). (Figure 4) The adhesion molecule CASPR/Paranodin/NCP1 (CASPR) is present on the axonal side and associates with neurofascin (Nfasc) 155 in the OL membrane for the purpose of adhesion (Tait et al.,

2000). The binding of CASPR to Nfasc 155 is essential for the formation of a structural component of the myelin-axon junction known as transverse bands. These "bands" provide the junction with a physical appearance that resembles invertebrate septate junctions which prevent free lateral diffusion of molecules along the membrane. When these junctions are compromised, both glial and neuronal protein domains are disrupted (Dupree et al., 1999; Bhat et al., 2001).

The proper functioning of the junction is crucial to maintaining axolemmal protein clustering. Although other factors may be involved (Kaplan et al., 1997), both initial clustering (Dugandzija-Novakovic et al.1995) and long-term domain maintenance (Dupree et al., 2005) both require physical contact between the glial cell and the neuron. Sodium and potassium channel clusters are maintained by these junctions and are easily studied via immunohistochemistry (IHC). Additionally, clustering of these channels is a valuable indicator of junctional integrity (Dupree et al., 1999).

Sodium channels are multi-domain membrane spanning proteins (Aidley, 1998) that provide the means by which sodium ions rapidly pass through the axolemma as action potentials travel down the axon. In the CNS two types of sodium channels (Nav1.2 and Nav1.6) have been found clustered at the node (Boiko et al., 2001; Kaplan et al., 2001). Nav1.2 is the immature form and is initially expressed in the CNS nodes of Ranvier. As myelination continues, Nav1.2 is replaced in over 90% of the CNS nodes by the mature form Nav1.6. Following a demyelinating event (Dupree et al., 2005) and in dysmyelinating animal models (Craner et al., 2003; 2004; Suzuki et al., 2004), Nav1.2

Figure 3: Sulfatide is synthesized from the addition of a sulfate group to galactocerebroside by the enzyme cerebroside sulfotransferase (CST). The galactocerebroside is synthesized by the addition of a galactose group to ceramide by the enzyme ceramide galactotransferase (CGT). (taken from Coetzee et al., 1998)

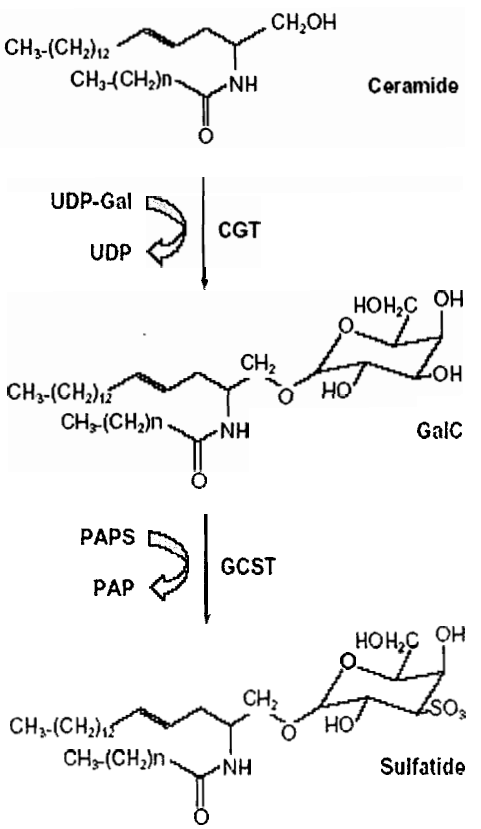

Figure 3: Synthetic pathway of sulfatide

Figure 4: (Upper left) A single PNS internodal segment is shown with the myelin sheath unwrapped. The segment is flanked by paranodes and nodes of Ranvier. (Upper right) an oligodendrocyte is shown with three processes terminating in three internodal segments, again with the myelin sheath unwrapped. (Below) An axonal node of Ranvier is shown in longitudinal-section. The three major regions are depicted: node, paranode, and internode. The juxtaparanode is the internodal region immediately adjacent to the paranode on the internodal side. As shown, sodium (Na+) channels cluster in the node, CASPR / Paranodin accumulates at the paranode, and rectifying potassium channels (Kv1.1 and Kv1.2) are concentrated at the juxtaparanode. (Taken from Dupree, 1996)

Figure 4: Nodal / Paranodal Region Architecture

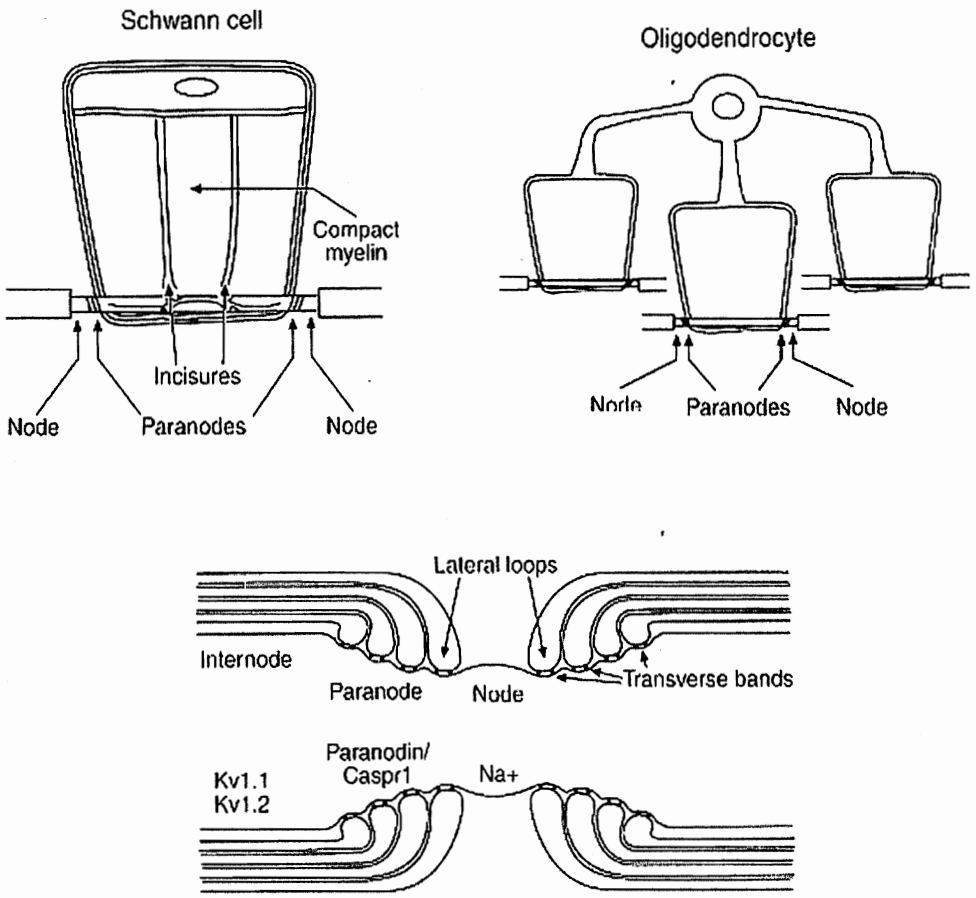

expression is significantly upregulated, suggesting that Nav1.2 may be used as a marker of de- and or dysmyelination.

CST Null Mouse

Work in an animal model demonstrates the critical role of ST in the maintenance of the paranodal region. Honke et al. (2002) engineered a CST null mouse in order to determine whether a single gene and enzyme were responsible for the production of ST. This mutant mouse displays minimal deficiencies through the early stages of development. By 6 weeks of age these animals exhibit profound motor dysfunction in their hind limbs accompanied by altered axo-glial interactions. These findings were confirmed by Marcus et al. (2006), who showed that the absence of ST does not result in the gross disruption of development, but that ST is essential for the maintenance of myelin and axon structure. In the aged CST null mouse, nodal structure is compromised, axon diameter is decreased, and neurons appear to be lost. Additionally, Ishibashi et al. (2002) reported that the initial clustering of K^+ and Na^+ channels was only mildly altered in the young ST null mice; however, with age and in the absence of demyelination, clusters of both the Na^+ and K^+ channels were lost, and K^+ channel clusters that remained were shifted to the paranodal region. In addition, CASPR was dispersed throughout the internode rather than clustered at the paranode. Taken together, these studies strongly suggest that ST is critical for the maintenance of neuronal membrane organization, function and even survival.

Proper localization of sodium channels to the node of Ranvier and potassium channels to the juxtaparanodal region are maintained by the integrity of the paranode. Is it possible to use this organization of protein domains, which is maintained by rafts and paranodal junctions, to measure changes in the interface between OLs and axons in AD. It is feasible to observe such modifications by uitilizing immunohistochemistry to visualize any rearrangement of Na^+ and K^+ channels in AD tissue.

Rationale and Hypothesis

The cause of NFTs and Aβ plaques, the hallmark AD pathologies, is not clear. Tangles and plaques are formed by enzymes that are preferentially sequestered to membrane domains called lipid rafts. Sulfatide is essential for the proper structure and function of lipid rafts. Our laboratory has demonstrated that reduced ST results in altered membrane domains that are normally maintained by adhesive contacts and functional lipid rafts. Sodium channel clusters at the nodes of Ranvier are lost as a result. This change in sodium channel localization provides a useful measure for assessing overall alterations in paranodal junctions and rafts. In this study, normal and age-matched AD brains will be immunolabeled in order to evaluate the amount of clusters present. I hypothesize that reduced ST in the AD brain disrupts lipid raft membrane domains as evidenced by loss of sodium channel clusters at the node of Ranvier.

Materials and Methods

Tissue Acquisition and Storage

Human brain tissue was acquired from the University of California at Los Angeles (UCLA) brain bank (Table 1). UCLA provided samples of occipital lobe. Tissue from severe AD, mild AD and non-AD patients (based on Braak and Braak staging) was requested, and 3 samples from each category were received.

The brain bank ranked each patient according to the Braak and Braak criteria and as cognitively normal or having dementia prior to death. The Braak and Braak stage refers to the presence and location NFTs in the post-mortem pathological analysis. Lower Braak and Braak scores (Table 1) correlated with 'no dementia' diagnosis, and higher scores with diagnosis of 'dementia.'

The brain bank provided information on the duration between death and collection of the tissue (ranging from 7 – 28 hours) although information for five of these samples was lacking. All samples were fresh frozen and shipped on dry ice. Upon receipt, the

Table 1: Information regarding the diagnosis of the patients and the post-mortem pathologic state of the tissue obtained. Time post-mortem refers to period between death and tissue collection. Braak and Braak stage was determined post-mortem primarily by the extent of NFTs.

Table 1: TISSUE INFORMATION (1 sample each: occipital lobe)

Sample	Diagnosis	Time Post-Mortem (Hours)	Braak & Braak Stage
20010036	CONTROL	9:00	CONTROL
20030024	CONTROL	22:00	CONTROL
20030021	AD-MILD	Not provided	II-III
20030018	AD-MILD	Not provided	III
20030028	AD-MILD	Not provided	III
20030017	AD-SEVERE	Not provided	VI
20030027	AD-SEVERE	Not provided	VI
20030030	AD-SEVERE	7:00	V

Reagents Used

Tissue sections were stained with Quickstain (American Master*tech Scientific, Inc.) in order to study the integrity of the tissue. The 1x phosphate buffered saline (PBS) used for IHC was composed of 160.1g NaCL, 28.8 g Na_2HPO_4, 4.8 g KH_2PO_4, 4.0 g KCl dissolved in 20L of filtered water and made at pH 7.4. In order to localize sodium and potassium channels, commercially available antibodies were used as previously described: pan Na channel antibody (Sigma S8809) (Dupree et al.., 1999; Marcus et al., 2001), Na channel Nav 1.2 (Upstate Biotechnology) (Dupree et al., 2005), and Kv1.1 potassium channel antibody (Upstate Biotechnology) (Dupree et al., 1999). To assure that the density of myelinated axons was comparable among samples, tissue sections were immunolabeled with antibodies directed against neurofilaments (SMI33, Covance Research Products) and the MT associated protein known as MAP1b (AA6, Sigma). An antibody against 2',3'-Cyclic nucleotide 3'-phosphodiesterase (CNPase, SMI91, Covance Research Products) was used to label myelin in order to distinguish between gray matter and white matter.

The standards for ST and cerebrosides were obtained from Avanti Polar Lipids (cat# 131305 [ST] and 131303 [Cerebrosides]). A protease inhibitor cocktail (Sigma cat# P8849) was used in the tissue homogenization process. Protein assay was performed using a BSA kit obtained from Pierce Biotechnology, Inc.

Tissue Handling

The fresh frozen tissue was immediately stored at -80° C upon receipt. The tissue was then slightly thawed in order to harvest small samples of WM enriched tissue that were embedded in OCT compound (Tissue-Tek, Optimum Cutting Temperature, Sakura Finetech). The OCT embedded tissue blocks were placed immediately on dry ice and again stored at -80° C. Each tissue block was then sectioned at a thickness of 10μm using a cryostat at -20° C. Twenty-five consecutive sections were placed on slides (ProbeOn Plus, Fisher), appropriately labeled (specimen#, brain region, section thickness, and slide order), and stored at -80° C.

Immunostaining protocol

Immunohistochemical staining was performed according to the method of (Dupree et al., 1999) Slides were removed from the freezer and allowed to air dry for 30 minutes. Excess OCT was cut away from the perimeter of the tissue. A hydrophobic barrier was applied around the section using a PAP pen (Super PAP Pen, Electron Microscopy Sciences) to assist in maintaining incubation solutions on the section. Dried slides were labeled to indicate antibody and incubated in -20° C acetone to permeabilize for 10 min. The slides were then rinsed three times in phosphate buffered saline (PBS) for five minutes each followed by a 30 minute incubation in a blocking solution. The blocking solution contained ~5% cold water fish skin gelatin (approximate since it was added dropwise and is extremely viscous, 10% fetal calf serum, and 0.1% Triton-X 100 in PBS. Following the block, sections were incubated in the appropriate primary antibody at the concentration

shown in Table 2. All antibodies used in this study have been well characterized in previously published studies from laboratory (Dupree et al., 1999; 2005; Marcus et al., 2002). The tissue remained in primary antibody overnight at 4° C in a humidified chamber to prevent drying. The following day, three PBS rinses and 30 min blocking steps were repeated, followed by a 90 min secondary antibody (Table 2) incubation in the dark at room temperature. The secondary antibodies, which were fluorescently conjugated, were also diluted in the blocking solution to a concentration of 1:200. The slides were then rinsed three times in PBS for 5 minutes and mounted with Vectashield (Vector Laboratories) medium and a cover slip was applied.

Controls, negative and positive

Mouse tissue was analyzed along with human tissue under the same conditions in order to confirm the specific binding of the antibodies. Since the specificity of the antibodies used have been established in mouse tissue, and labeling patterns were consistent between the two animals it was concluded that binding in the human occurred and was specific. Labeling with different primary antibodies and the same secondary revealed unique patterns of labeling and therefore assured the specificity of each. This provided both positive and negative controls for the primary antibody. Tissue was also stained with primary antibody and no secondary to ensure that the primary antibody did not fluoresce. In order to confirm that the secondary antibodies only bound to the primary antibodies used, IHC was performed in the absence of any primary antibody under identical conditions.

Table 2: Primary and Secondary Antibodies Used

Table 2: Primary Antibody Concentrations and Corresponding Secondary Antibodies with Conjugated Fluorochromes

Primary Antibody	Pan NaCh	Kv1.1	MAP1b	NaCh 1.2	Neurofilament	CNPase
Dilution	1:100	1:100	1:100	1:100	1:1000	1:1000
Secondary Antibody (1:200)	Alexa 594 Anti-Mouse	Alexa 594 Anti-Mouse	Alexa 594 Anti-Mouse	Alexa 594 Anti-Rabbit	Alexa 594 Anti-Mouse	Alexa 594 Anti-Mouse

Analysis of Sodium Channel Clusters

Quickstain

Each sample was stained with Quickstain in order to confirm the integrity of the tissue. Tissue was analyzed for presence or lack of artifactual spaces. White matter without significant space was deemed appropriate for IHC. One drop of dye was placed on a tissue section for ten seconds and then rinsed in phosphate buffered solution (PBS) for 10 seconds. Slides were dried and cover slipped with immersion oil. Slides were visualized under a Nikon Eclipse 800M bright field microscope and images were recorded at the GM / WM interface at 40x and at 200x in each of the two regions (GM and WM). Representative fields for each tissue section were chosen and recorded. Consecutive sections were analyzed by Quickstain and by IHC for NaCh clusters.

The first step in analyzing each slide was to distinguish between WM and GM. Prior to nodal/paranodal protein data collection, myelin markers were used for this purpose (as previously discussed). In addition to the myelin antibody markers, distinct patterns of lipofuscin (LF), corresponding to the WM and GM region, was observed. Subsequently, LF patterning was used to make the distinction.

Confocal Microscopy

After confirming areas, of white matter, all sections were imaged using the Leica TCS SP2 AOBS or Zeiss LSM510 NLO META confocal microscopes housed in the VCU Microscopy Facility. A minimum of six fields were collected, depending on the size of the WM region in each sample. In all cases, except for Kv1.1 data collection, a single optical plane was scanned. In the case of the Kv1.1, a maximum projection of a z-stack of 10 optical planes at a step size of 0.4 μm was collected in order to capture pairs of potassium channel clusters in different planes. Gain and offset settings were held as consistent as possible from frame to frame. Following is a list of settings used for image collection (Table 3).

Digital Removal of Autoflourescence

One of the difficulties of fluorescent labeling of human tissue is the presence of the auto-fluorescing substance known as lipofuscin (LF). LF accumulates in cell bodies and is composed of lipids, metals, organic molecules, and biomolecules (as reviewed by Brunk and Terman, 2002). LF emits fluorescence in the red spectrum when excited with 488 and 594 nm light. The majority of the experiments were performed with a secondary antibody that was optimally excited at 594 nm and which also emitted light in the red spectrum. Since both the fluorescent label and LF emitted in the same region of the spectrum, it was not possible to discern specific labeling from LF autoflourescence. Two techniques were employed to resolve this issue. On the Leica confocal microscope, a subtraction technique was used.

Table 3: These settings were determined to be optimal for the information desired.

Table 3: Confocal microscope settings

	Gain	Offset	Pinhole Diam.	Zoom	Objective	Format	Line Av	Voxel Size
Leica	700 +/- 71	0 +/- 0.05	115 µm = 1 Airy Unit	2	63x	1024 x 1024	4	116.14 x 116.14 nm
Zeiss	700 +/- 63	0 +/- 0.05	112 µm = 1 Airy Unit	2	63x	1352 x 1352	4	98.82 x 98.82 nm

Briefly, when excited by the 488 nm laser, only LF fluorescence was present, and thus all pixels visible in this image corresponded to LF. Another image was taken under 594 nm light that contained specific labeling for the antibody used as well as LF autoflouresence. All pixels from the 488 image were subtracted from the 594 image leaving only pixels corresponding to the protein of interest. The subtraction method was not ideal, however, since in the instance of pixels that overlapped between the two channels, the signal of the desired channel was diminished or eliminated.

In addition to the subtraction method, autoflourescence and antibody labeling were also distinguished by the Zeiss spectral unmixing capabilities of the META system of the Zeiss confocal microscope. With the exception of the neuronal markers to neurofilaments and MAP1b, used to determine axon density, all of the IHC experiments were completed on the Zeiss confocal microscope in order to use its META capabilities. Since only ratio between the clusters (measured on the Zeiss) and axon density (measured on the Leica) was needed, data from one microscope could be used to analyze data from the other. The META detector was a polychromatic 32-channel detector for fast acquisition of lambda stacks and allowed simultaneous acquisition of up to 8 channels. Multiple images of the same field were gathered - each scanned using incremental emitted wavelengths from 447-704 nm. These data were compiled in order to create profiles of the fluorescing intensity for each emitted wavelength at each pixel. The profiles were curves plotted with fluorescent intensity on the y–axis and the spectrum of emission wavelengths on the x-axis.

Profiles of specific pixels were then chosen as representative of each fluorescent species (i.e. 594, lipofuscin, background). All signals that identified with profiles for LF and background were digitally removed from the image. Thus, only pixels corresponding to the 594 fluorochrome (which was conjugated to the secondary antibody and corresponded to the immunolabeled protein of interest) remained in the recorded image. This procedure, called linear unmixing, was a more precise method of identifying which pixels correspond to specific secondary antibodies since it was able to distinguish even between overlapping pixels based their the spectral fingerprints (Figure 7).

Quantitation of sodium channel clustering

Following spectral unmixing, the clusters of sodium and potassium channels were counted with IPLAB (Scanalalytics, Inc) software using segmentation analysis. The threshold was set such that the number of clusters counted for several fields corresponded approximately to the numbers generated by counting manually. In the cluster counts IPLAB's segment quantification feature was used with settings including pixels with intensities between 50 and 255 and clusters having areas of between 9 and 1000 pixels (9,800 nm^2 / pixel). The threshold (intensity) and cluster size settings were optimized in an attempt to reproduce the choices made by eye as to what constituted a cluster and to reproduce manual counts. These setting were chosen by first counting several different frames manually. The same frames were then subjected to quantification analyses with various combinations of intensity threshold and number of pixels per cluster settings. The optimal settings were chosen when the clusters outlined by the software resembled the

shape and size of those seen in the raw images and the numbers of clusters counted by IMAGEJ (http://rsb.info.nih.gov/ij/) were similar to those that were manually obtained.

To assure comparisons of structurally similar brain regions, axon fiber densities were calculated using axonal markers based on percent labeled pixels per field. As previously indicated, an antibody to MT associated protein 1b (MAP1b), which is a good indicator of axonal MTs, was used as well as an antibody directed against neurofilaments. For this quantification, Image J software was utilized to count all pixels in a field that had intensities between 70 and 255 on the thresholding feature of the software. This range was chosen by simultaneously viewing thresholded and original images to create and image which only revealed pixels pertaining to axons. Sodium channel clusters were counted and then standardized based on the obtained axon densities. Cluster counts were divided by axon densities generating numbers in clusters / μm^2 of axon / field.

Statistics

One section of each sample was analyzed. Every ninth field was recorded such that a minimum of six fields analyzed depending on the amount of WM per sample All values are presented as mean +/- standard deviation (SD). All data were statistically analyzed by t-test or analysis of variance (ANOVA) where appropriate, using Sigmastat software package (Systat Software Inc.) with the assistance of Dr. David Simpson, Associate Professor of Anatomy and Neurobiology at VCU. Significance was set at $p < 0.05$.

Thin layer analysis of sulfatide content

Lipid Extraction

Lipids were extracted as previously published by Sato and Yu (1990). Dr. Carmen Sato-Bigbee, Associate Professor of Biochemistry and Emilse Sanchez guided this portion of the study and all TLC procedures were conducted in Dr. Sato-Bigbee's laboratory. Briefly, for the extraction, 110mg of WM enriched samples were harvested (confirmed by visual inspection). For each specimen, the tissue sample was homogenized in 500uL of PBS that contained a protease inhibitor cocktail (Sigma cat# P8849) on wet ice. An aliquot of homogenate was set aside at 4° C for protein analysis. A 200uL aliquot of the homogenate was added to 40 volumes of choloroform:methanol 2:1. All of the steps after homogenization were performed at room temperature. Each sample was then centrifuged at 2000 rpm for 10 min. The supernatant was transferred to a fresh 15ml plastic graduated tube (Falcon, Fisher Scientific). Distilled water in the amount of 20% of the original solvent volume was then added. The sample was shaken, allowed to settle, and centrifuged at 1000 rpm for 5 min. The top of the upper layer (the aqueous phase) was marked on the tube and the upper layer was removed. The tube was filled to the mark with Chloroform:Methanol:Water (4:48:47). The sample was shaken, settled, and centrifuged at 1000 rpm for 5 min. The upper 2 layers, the aqueous and interphase, were removed and the sample was dried under nitrogen in order to prevent oxidative degradation. The sample was then resuspended in chloroform:methanol 2:1 in 20% of initial solvent volume. After the extraction, volumes of the organic layer, which

contained the lipids, varied, suggesting that water content varied among the samples. These volume values were used later to standardize the TLC results.

To determine which bands correlated with ST, cerebroside and ST standards were run next to samples on the TLC plate. The standards for ST and cerebrosides were obtained from Avanti Polar Lipids (cat# 131305 [ST] and 131303 [Cerebrosides]). Stock solutions of standards were at 1.7 μg/μL in 2:1 chloroform:methanol.

Preparation of tissue

Optimal loading amount of the sample was predetermined for GM and WM based on a TLC of a series of increasing amounts of lipids. Loading volumes were made by pipetting various masses of total lipids into disposable glass culture tubes (Baxter 12x75mm) and drying under nitrogen. Samples were then redissolved in 10 μL of 2:1 Chloroform:Methanol, the optimal TLC loading volume as previously determined by (Sato and Yu, 1990). The samples were cortical regions enriched in WM (110mg). The mass of the human samples was chosen based the amount of WM available. A TLC of a series of amounts of lipids (Figure 12) was performed on non-diseased WM and GM samples at concentrations: 5, 10, and 20 μL (dried under nitrogen and redissolved in 10 μL of choroform:methanol). The 5uL band was too faint and the 10 μL band too large (Figure 13). Therefore, 7.5 μL was determined to be the optimal load for WM. One and three μL volumes of standards (1.7 ug / μL) were diluted to 10uL and loaded.

TLC Plate loading and developing

The TLC protocol was as follows: The silica gel plate (obtained from EMD Chemicals cat# 11764/6) was activated by heating at 130° C for two hours. The samples were immediately loaded on the plate on 1.0 cm lines spaced 0.5 cm apart. The material was loaded 1.5 cm from the bottom of the plate to ensure that the solvent in the TLC well did not contact the sample. A 25mL Hamilton glass syringe with a blunt tip was used for loading. Samples were added dropwise. The plate was placed vertically in the well such that less than 1.5 cm of the plate was immersed in the solvent solution of methyl acetate:chloroform:methanol:1-propanol:water (25:28:10:25:7) and the well was sealed. The samples were allowed to run until the progress of the mobile phase had visibly ceased to progress. The plate was stained with orcinol which has been shown by Zoller et al. (2005), to be especially effective in staining ST and the images were recorded with a Fluorochem Imaging system (Alpha Innotech)

Protein Assay

In order to further standardize our TLC data, a protein assay was performed. Aliquots of the tissue homogenate were used to determine the total concentration of protein in the sample. 300uL of the initial 500uL homogenate of the tissue samples was used for the assay. This volume was diluted with 1mL of radioimmunoprecipitation (RIPA) buffer solution and further homogenized in a 15mL disposable tissue grinder (VWR International, 47732-446). RIPA buffer was added to reach a dilution of 1:20 of the original 300μL aliquot. The tissue was further homogenized in a glass tissue grinding

tube with a ceramic pestle bit in a ring-stand mounted drill. The sample was then assayed for total protein content at several dilutions. The assay used was a Pierce BSA kit that measures total tryptophan residues. The assay was performed on each sample in triplicate along with a standard curve using bovine albumin. Protein concentrations were measured using an ELISA plate reader at 570 nm.

Quantification of TLC's

The densities of bands were measured with ImageJ image analysis software. Densities were calculated by selecting the combined hydroxylated and non-hydroxylated ST bands and calculating the area under the peaks in curves corresponding to the bands. From the densitometry data, a total number of optical density units for the entire 110mg tissue sample was extrapolated. Considering that the number of OD units for the ST bands for a given lane correspond to the amount of ST in volume of lipids loaded, a concentration in the form of OD units per mL of lipid extract can be calculated. Using the fraction of the homogenate which the lipid extract constitutes, OD units per mL of homogenate can be calculated. Since the tissue was homogenized in 500mL of PBS, multiplying the OD units of ST / mL homogenate by 500 will give total OD units of ST for the tissue sample. A total amount of protein (in mg) for the harvested sample was calculated. A standard curve was generated from the ST standards of known concentration versus optical density enabling the conversion of the density of ST in the samples to be converted to mass. The densities of the ST bands were standardized relative to the cerebroside and cholesterol lipid bands as well as to total protein content.

Results were reported as μg ST / μg protein and μg ST / μg cerebroside. A one-way ANOVA among the sample groups was performed on the standardized values for ST content.

Results

Immunohistochemistry

Immunohistochemistry (IHC) techniques were employed to evaluate the competency of the axo-glial interactions in the AD tissue based on the clustering of sodium channels. For these studies, fresh frozen tissue samples were immunolabeled for several paranodal and nodal proteins known either to mediate axo-glial interactions or whose distribution is directly altered when these mediations are compromised (Menegoz et al., 1997; Dupree et al., 1999; Rios et al., 2000; Ishibashi et al., 2002).

Tissue samples

Quickstain analysis revealed that the WM of the most samples was in tact (Figure 5). Some holes were present in GM, though minimal. Only those tissues which were judged to be in good condition were used.

Gray and white matter regions determined by myelin markers and lipofuscin patterns

As shown in Figure 6, distinct patterns of lipofuscin exist for gray matter and white matter. These regions were initially determined by myelin markers. CNP was used as a myelin marker and provided very clear visualization of distinct GM and WM regions. CNP labeling confirmed that the distinct patterns of autofluorescence was a reliable method of differentiating GM and WM regions.

Axonal orientation and girth consistent among samples

First, to assure that the density of myelinated axons was comparable among samples, tissue sections were immunolabeled with antibodies directed against neurofilaments (SMI33, Covance Research Products) and the MT associated protein known as MAP1b (AA6, Sigma). An antibody against 2',3'-Cyclic nucleotide 3'-phosphodiesterase (CNP) was used to label myelin in order to distinguish between GM and WM.

Using qualitative assessment, it was determined that the regions analyzed contained homogenous populations of axonal processes with respect to caliber and density. Due to the fact that the qualitative analysis showed uniformity among samples and that most of the axons in all samples were in oblique section, density was determined to be a reliable correlate to axon length. Since the number of clusters is dependant on axon length, the cluster counts were standardized based on axon density. In other words, the number of ion channel clusters per field was divided by the density of axonal staining per field.

Figure 5: Samples were stained with Quickstain to assess degree of artifact. Images shown are representative of condition of the typical sample. What little artifact is present is in the form of spaces within the tissue as shown by the arrows, which is probably due to freezing. Typical fields of A) GM, B) WM. The GM regions consistently show greater artifact than WM.

Figure 5: Typical Tissue Samples Show Only Minor Artifact

A) Gray Matter

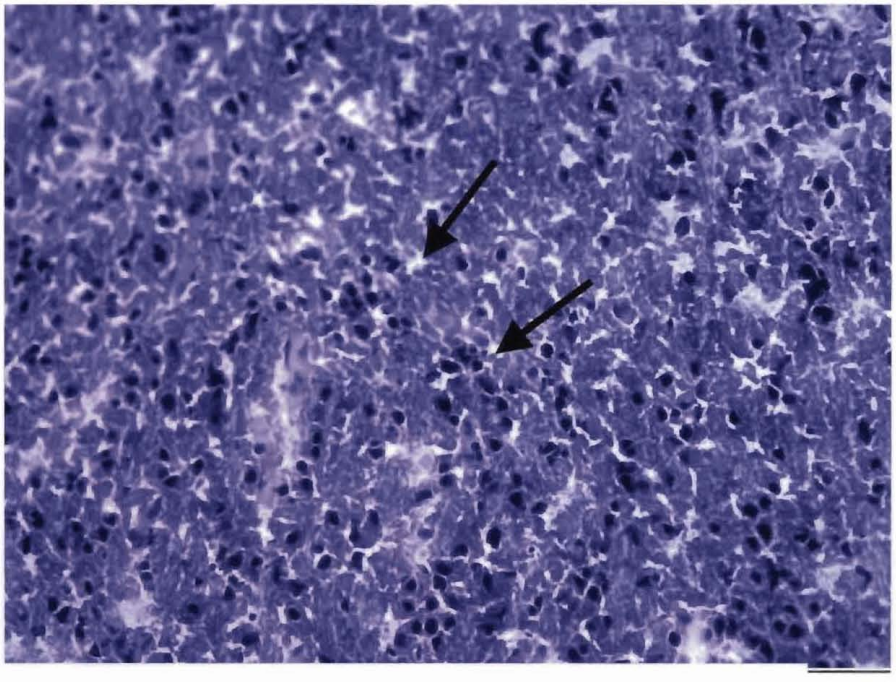

B) White Matter

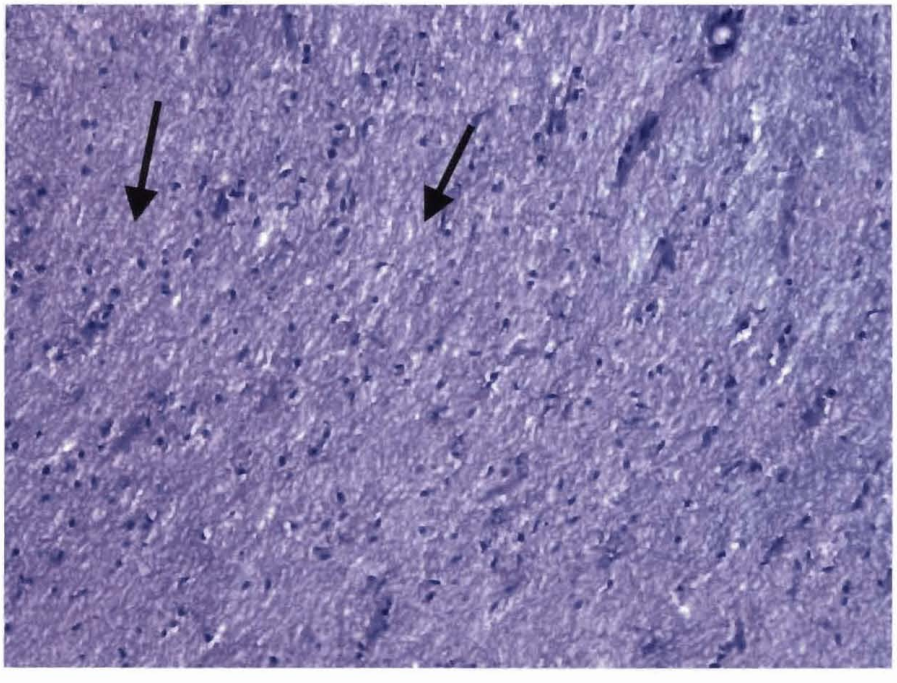

Figure 6 a, b: a) GM exhibits larger clusters of lipofuscin autoflouresence yet the clusters are less uniform in distribution, shapes and sizes compared to b) WM which lacks neuronal cell bodies and thus smaller clusters of LF are observed in a more regular pattern. Neither (a) nor (b) were treated with primary antibody, but were otherwise subjected to the identical protocol as the other IHC experiments, and thus no specific immunolabeling is present in these images.

Figure 6 a, b: Lipofuscin patterns used to differentiate gray and white matter

a) Gray Matter

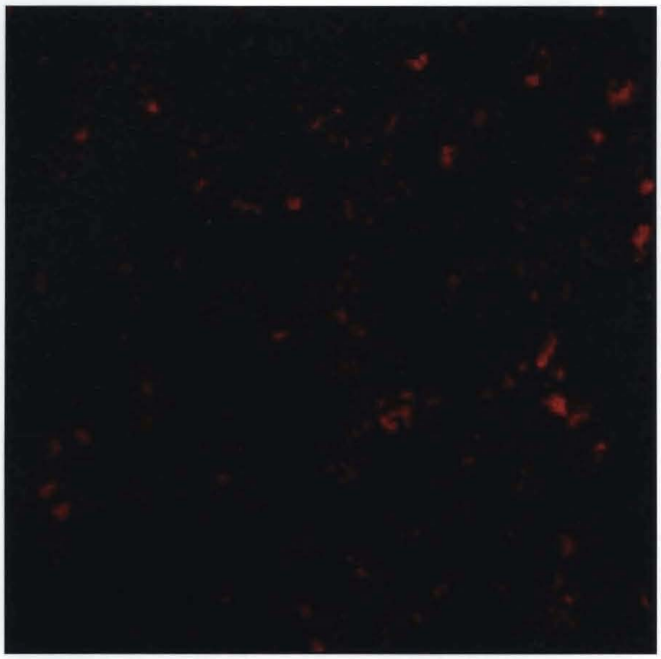

b) White Matter

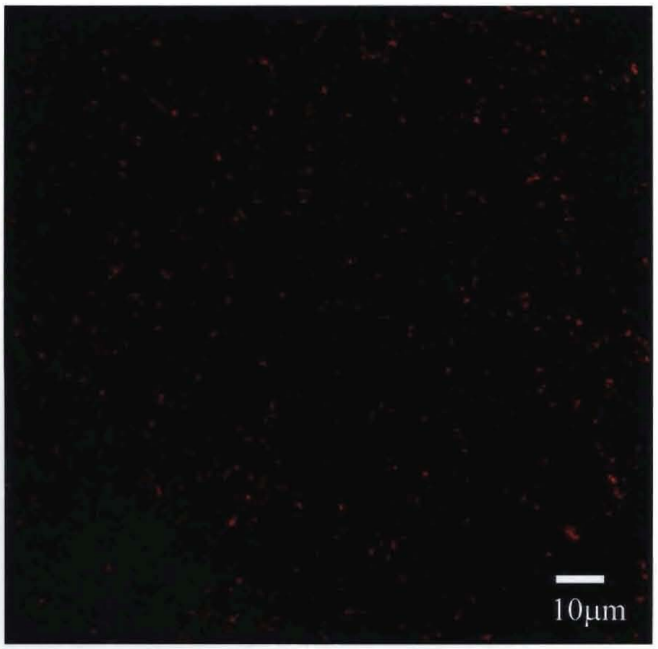

Figure 7 a, b: a) Lipofuscin (yellow) makes sodium channel clusters (white) difficult to identify. b) Lipofuscin signal has been removed via lambda scanning and linear unmixing.

Figure 7: Lipofuscin removal made sodium channel cluster identification possible

a) Pan NaCh labeling with lipofuscin

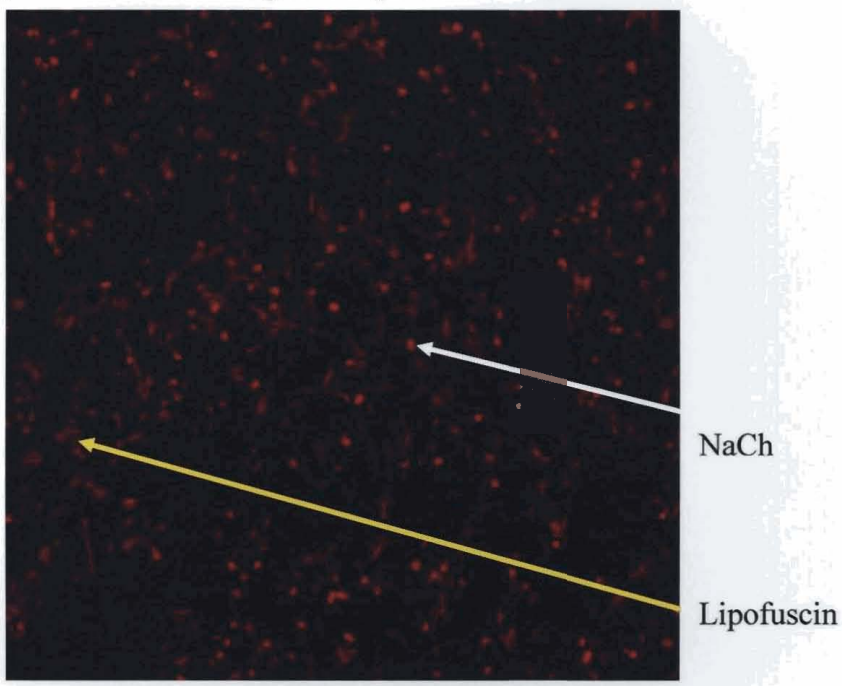

b) Pan NaCh Labeling without lipofuscin

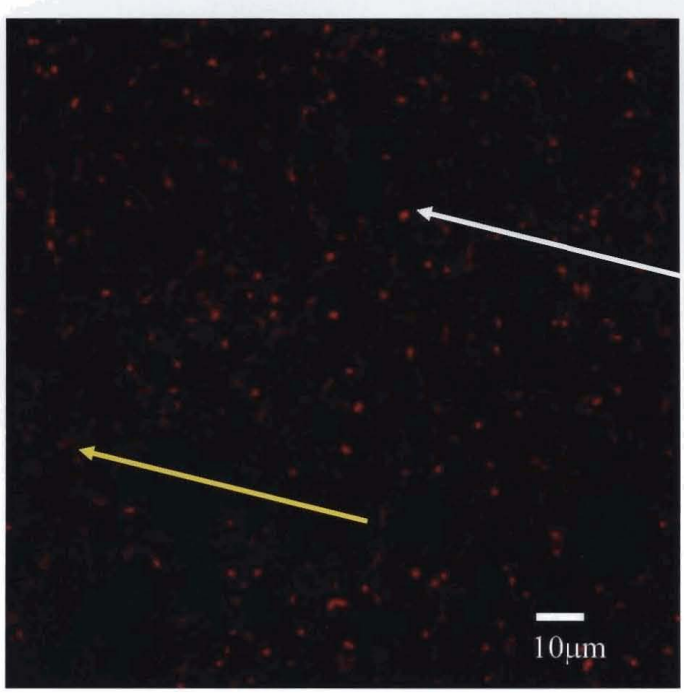

Axonal markers revealed slight variations in axon densities

Axonal markers to MAP1b and neurofilaments were used to compare relative axon densities between brain regions. Both qualitative and quantitative assessments were used to compare tissue samples. Among the samples, axon girth appeared constant; few axons were longitudinally oriented; most axons were transversely or obliquely oriented. The results from this analysis are shown below in Table 4 and Figure 8. These densities were used to standardize the protein clustering values. MAP1b yielded a mean axon density of 217 +/- 105 pixels/field for severe AD, 200 +/- 105 for mild, and 173 +/- 19 for non-AD with a p value of 0.9. Neurofilament densities were 186 +/- 75 for severe, 143 +/- 23 for mild, and 174 +/- 36 for the control and a p value of 0.6.

Nodal architecture was intact

IHC studies on the ST null mouse revealed dramatic alteration in protein clusters (Ishibashi et al., 2002). To test whether the nodal changes seen in the ST null mouse were also present in AD, the distribution of several CNS nodal and paranodal proteins was determined. Negative control labeling with secondary antibodies in the absence of primary antibodies revealed no specific labeling.

Sodium channels were unchanged between sample groups

In the non-standardized cluster counts from the pan NaCh there was no significant difference between AD and non-AD as seen in Table 5 and Figures 9, 10, and 11. Age-

Figure 8: Variability in axonal labeling among samples: Samples were labeled with antibodies directed against axonal cytoskeleton in order to calculate axon density

Figure 8 a, b, c, & d: Variability in axonal labeling seen among samples

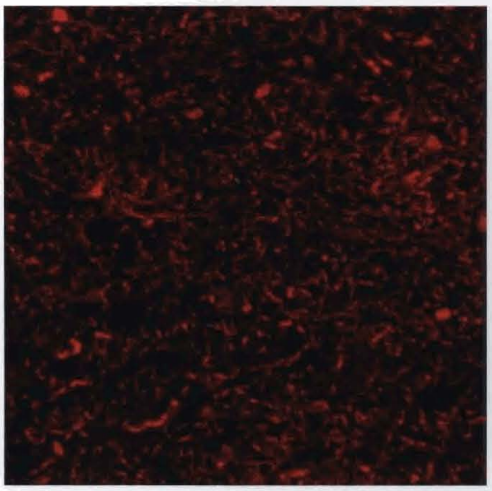

a) non-AD Neurofilament

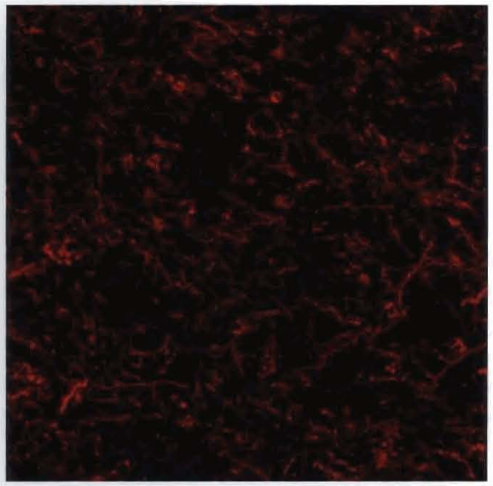

b) non-AD MAP1b

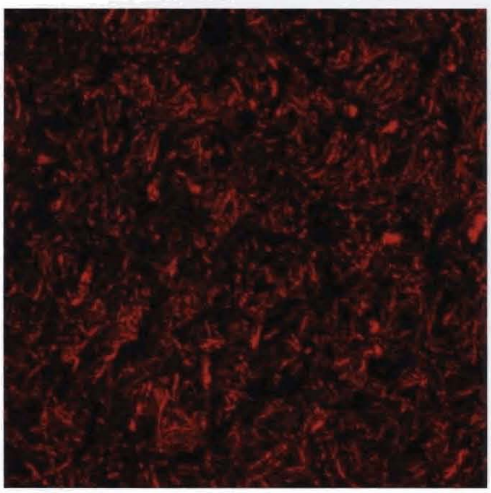

c) AD Neurofilament

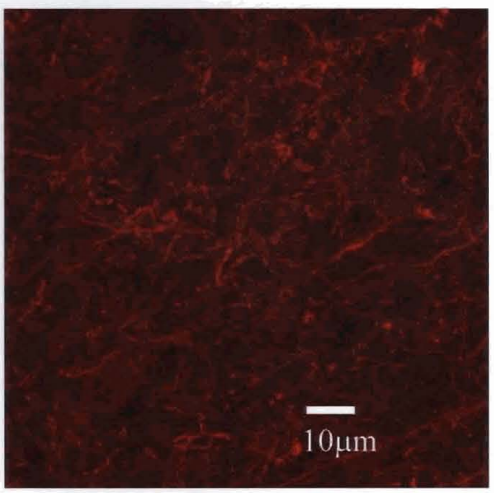

d) AD MAP1b

Table 4: Axon densities were measured in number of pixels per frame of labeling for Map1b and neurofilaments above an intensity of 50 (on a scale of 0-255). Means and standard deviations are given for each disease or non-disease group.

Table 4: Axon densities varied among samples

Map1b	Sample	Area	Mean	SD
Severe AD	20030030	336	217	105
	20030017	136		
	20030027	178		
Mild AD	20030021	115	200	105
	20030028	317		
	20030018	169		
Non-AD	20030024	160	178	18
	20030036	195		
Neurofilament				
Severe AD	20030030	217	186	75
	20030017	100		
	20030027	241		
Mild AD	20030021	118	143	23
	20030028	163		
	20030018	149		
Non-AD	20030024	215	185.5	29
	20030036	156		

Figure 9 a, b: Pan NaCh Labeling Unchanged Between Non-Alzheimer's and Alzheimer's Tissue These figures demonstrate the clustering seen in sodium channels at the nodes of Ranvier. Mouse monoclonal pan NaCh primary antibody was used at 1:100; Alexa 594 conjugated anti-mouse secondary antibody at 1:200.

Figure 9: Pan Sodium Channel Labeling Unchanged

a) Non-Alzheimer's Pan NaCh labeling

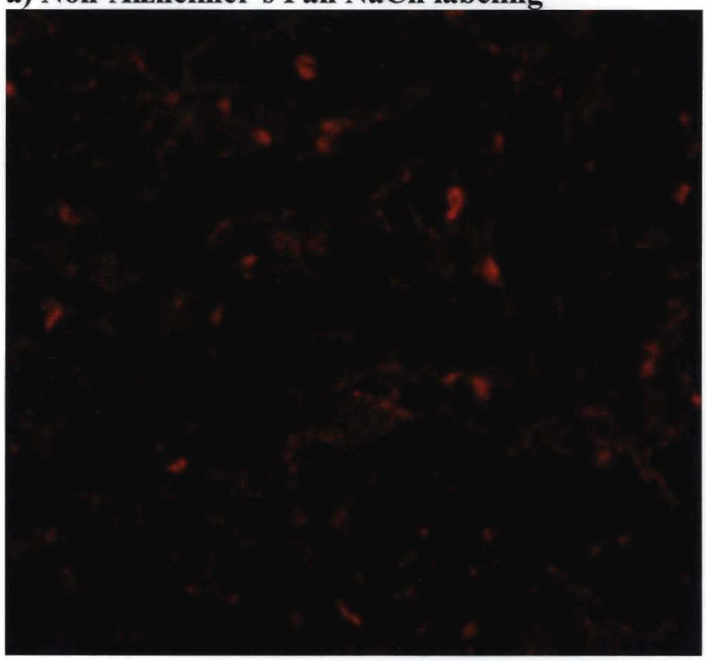

b) Alzheimer's Pan NaCh Labeling

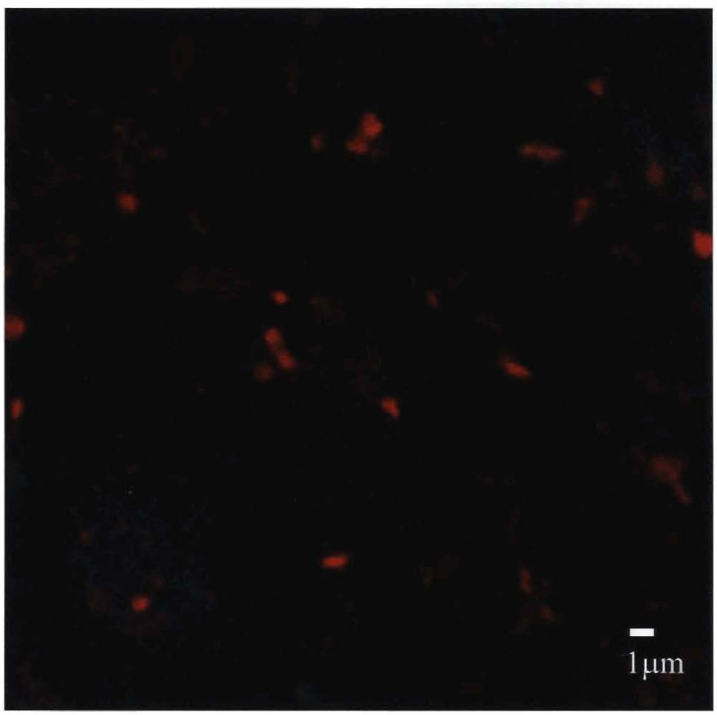

matched, non-demented brains revealed the same cluster mean (329 +/- 68 clusters/field) as the severe diseased (308 +/- 170 clusters/field) and the mild diseased (281 +/- 104) brains. When standardized against axon density (Figure 11), the pan NaCh antibody again revealed no significant difference (P = 0.235) among the sample groups as determined by aone-way ANOVA. Raw and standardized means among groups showed similar trends.

Nav1.2 sodium channels unchanged

Despite the fact that the pan NaCh antibody showed no difference between sample groups, it remained to be determined whether clustering of specific Na channel isoforms was altered. Quantification of the clustering of Nav 1.2 removed this ambiguity as well as serving as a marker for demyelinating pathology. This antibody revealed no significant difference (P = 0.142) between AD and non-AD groups for either clusters or total area (Table 6). It was therefore concluded that there were no differences between these sample groups for the Nav 1.6.

Thin Layer Chromatography

No Difference in ST Levels Among Samples

Considering the premise of the study was the previous findings of Gottfries, Karlsson, and Svennerholm (1996), and more recent data from Han et al. (2002), who reported a 60% decrease in WM ST, TLC was employed to confirm these results. Upon

Figure 10: Shown in purple are the average number of total pixels per field of MAP1b labeling (representing axon density). In red are the average number of clusters of sodium channels per field. The first three pairs represent severe AD, the second three, mild, and the third, non-diseased. This figure demonstrates how the axonal marker MAP1b and NaCh clustering varied in parallel with each another.

Figure 10: NaCh Clusters and MAP1b Pixels

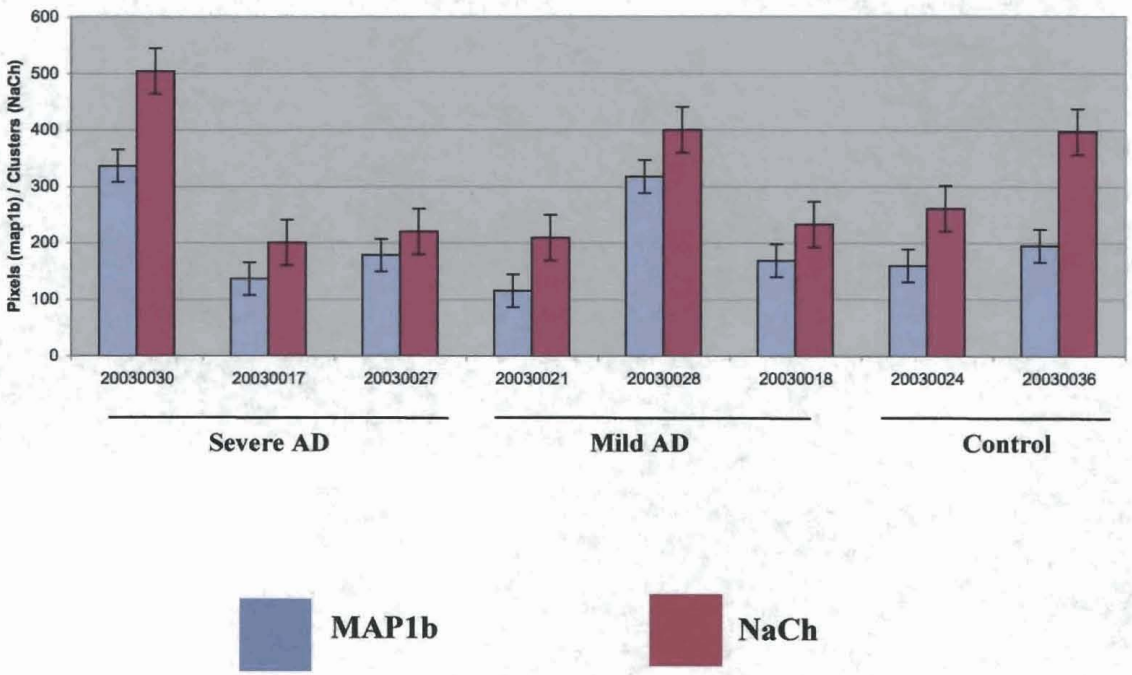

Figure 11: This figure shows the mean number of clusters per field divided by the mean axonal density as determined by MAP1b immunolabeling. A slight trend can be detected in this graph, though an analysis of variance revealed any differences to be insignificant.

Figure 11: No Difference in Sodium Channel Clusters Standardized with MAP1b

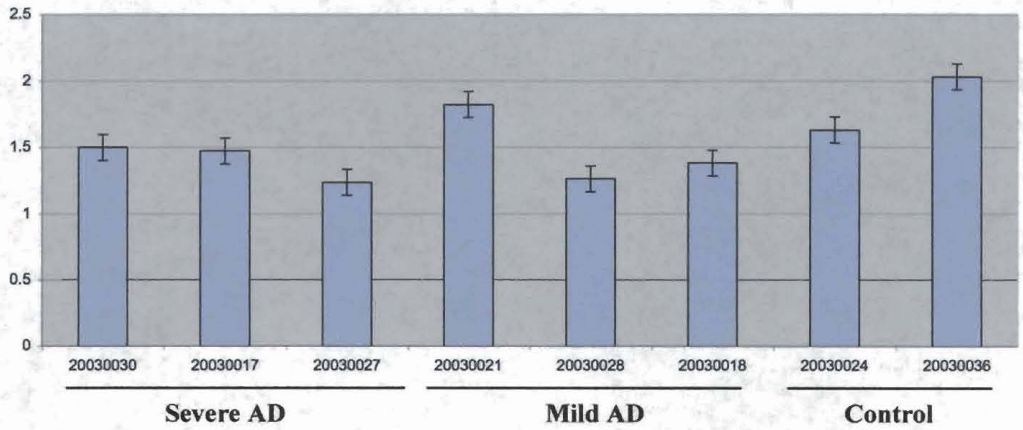

Table 5: This table contains mean number of clusters per field for NaCh for the three sample groups of the tissue in the 'NaCh' clusters columns. Columns headed 'NaCh' / MAP1b' or SMI 33 show cluster counts standardized by dividing by axon density.

Table 5: No Difference in Sodium and Potassium Channel Clusters

	Sample	NaCh Clusters	NaCh / MAP1b	NaCh / SMI 33
Severe	20030030	503	1.50	2.32
	20030017	200	1.47	2.00
	20030027	220	1.23	0.91
Average		308	1.40	1.74
SD		170	0.15	0.74
Mild	20030021	209	1.82	1.77
	20030028	400	1.26	2.45
	20030018	233	1.11	1.25
Average		281	1.40	1.83
SD		104	0.38	0.60
Control	20030024	261	1.63	1.21
	20030036	396	2.03	2.54
Average		329	1.83	1.88
SD		68	0.28	0.67

initial inspection by eye, there appeared to be no difference among sample groups (Figure 13). Densitometry with ImageJ analysis software revealed that there was a trend towards a decrease in ST in the AD groups although the differences were not significant. One TLC was preformed and densitometry was performed on one band of each sample. In the analysis ST levels were determined to be slightly higher in the control group than in the mild and severe AD groups (Table 7, Figure 13). The control group revealed 0.48 +/- 0.05 μg ST / OD units of cholesterol compared to the mild group, which presented a ratio of 0.36 +/- 0.01. Similarly the severe group exhibited a ST to cholesterol ratio of 0.36 +/- 0.07. A one-way ANOVA gave a P-value for these three groups of 0.201.

Table 6: Shown are total segments/field and areas/field of labeling of anti-Nav1.2 primary antibodies in the tissue

Table 6: No Difference in Sodium Channel 1.2

	Sample	Nav1.2 Clusters	Nav1.2 Area
Severe	30	100	9436
	17	120	15372
	27	234	36872
	Average	151	20560
	SD	72	14435
Mild	21	73	7959
	28	152	19955
	18	88	6728
	Average	104	11547
	SD	42	7307
Control	24	98	12155
	36	105	13245
	Average	102	12700
	SD	4	545

Figure 12: This figure shows from left to right – two lanes of cerebroside standards: 0.02 and 0.06 μg; two lanes of ST standards (2 bonds: non-hydroxylated above hydroxylated) 0.02 and 0.06 μg; three lanes of WM enriched non-diseased human brain extract: 5, 10, 20 μL of extract; and three lanes of GM at 5, 10 and 20uL of extract. Nothing was loaded on the empty lane between the 5 μL and 10 μL GM.

Figure 12: 15µL Determined Optimal Loading Volume for White Matter

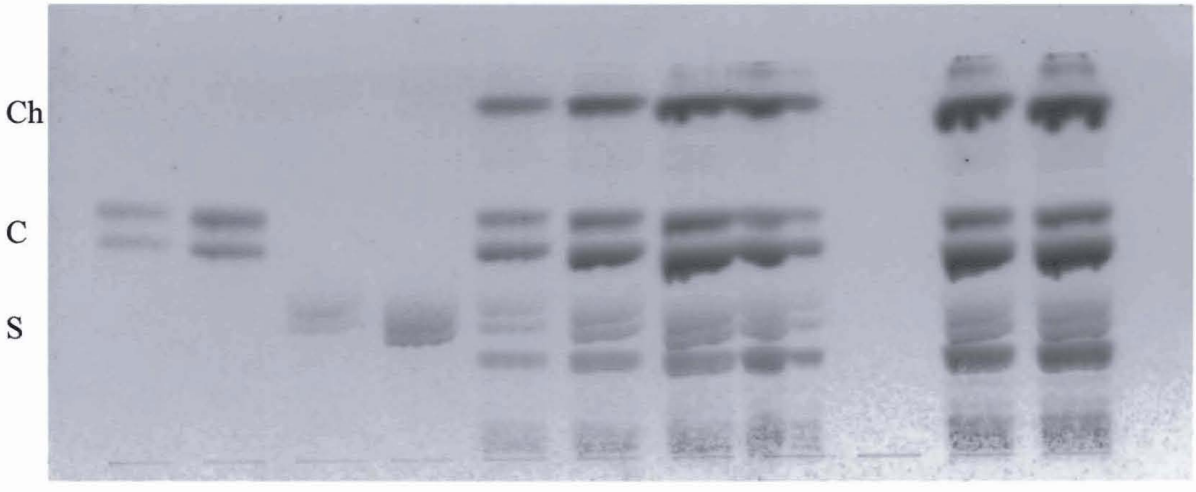

Figure 13: The TLC shows the various lipid bands found in the white matter enriched human brain tissue samples. The top band is cholesterol (Ch), the next two bands are cerebrosides (non-hydroxylated above hydroxylated) as can be seen by the cerebrosides (C) standard bands seen on the left. The next two bands correspond to ST (non-hydroxylated above hydroxylated) as seen in the (ST) standards the left.

Figure 13: No Change in White Matter Sulfatide Levels Among Sample Groups

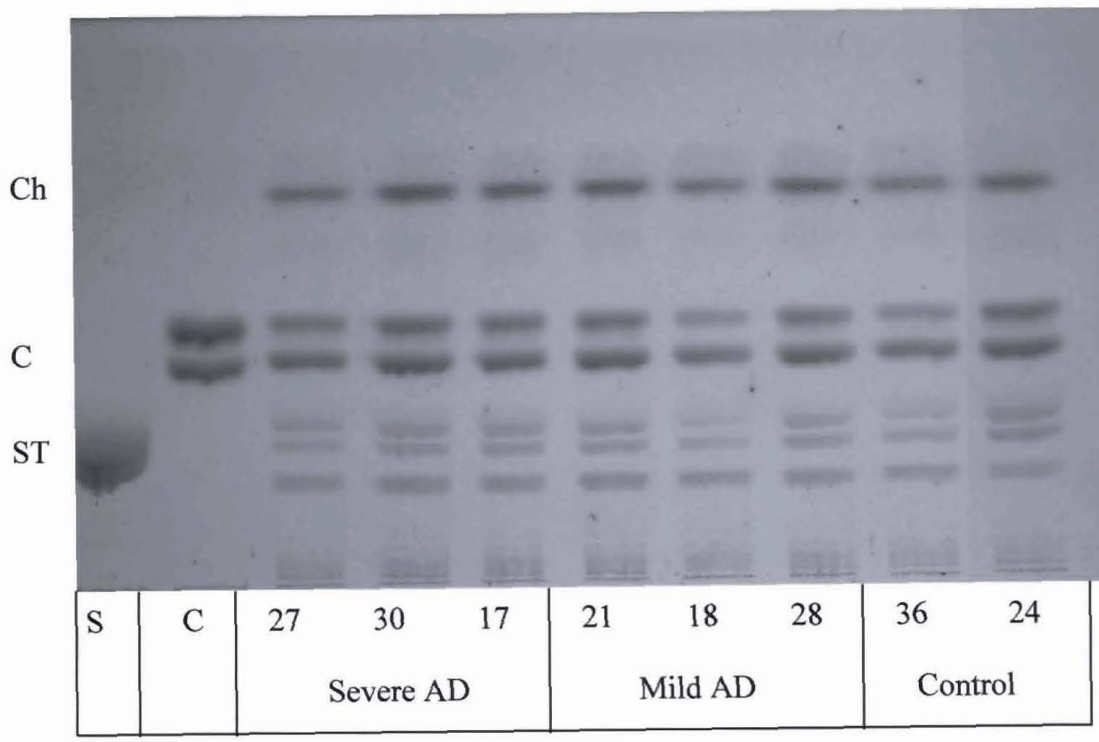

Table 7: Shown are the standardized optical densities of the ST bands from TLC analysis of the tissue. The ST was standardized by the cholesterol band as shown in the 'ST / cholesterol' column. ST was also standardized by protein.

Table 7: No Difference in White Matter Sulfatide Levels

	Sample	μg ST / μg Cholesterol	μg ST / μg Protein
Severe	27	0.36	48
	30	0.29	81
	17	0.43	62
	Mean	0.36	64
	SD	0.07	8
Mild	21	0.37	62
	18	0.34	78
	28	0.37	40
	Mean	0.36	56
	SD	0.01	15
Control	36	0.43	38
	24	0.53	86
	Mean	0.48	62
	SD	0.05	20

DISCUSSION

Alzheimer's disease is characterized by accumulation of Aβ plaques, NFTs and neuronal death, though the cause of these hallmark pathologies remains unclear. Enzymes that are involved in the formation of Aβ plaques and NFTs are associated with the neuronal membrane (Kramer et al., 1999; Ehehalt et al., 2003), and proper partitioning in the normal membrane prevents inappropriate interaction of axolemmal enzymes and potential substrates (reviewed by Simons and Ikonen, 1997). Sulfatide is essential for the proper structure and function of lipid rafts, and Han et al. (2002) recently reported that ST is significantly reduced even in the earliest stages of AD. Thus, I hypothesized that reduced ST in the AD brain would disrupt lipid raft membrane domains as evidenced by loss of sodium channel clusters at the node of ranvier. In the present study, membrane domain organization appeared to be in tact in AD tissue. Sulfatide levels also appeared to be unchanged. I was therefore unable to support my hypothesis.

Protein Organization

Sodium channel clustering was used as a marker to determine membrane domain organization since it is well characterized and easily labeled. Clusters were unchanged in AD tissue at both early and late stages as compared to controls.

Simons and Ehehalt, 2002 and Ehehalt et al., 2003 suggested that rafts are involved Aβ formation. When cholesterol was depleted Aβ generation increased and α-cleavage (non-amyloidegenic) increased. Cholesterol depletion would disrupt raft organization and render more of the usually raft associated APP in non-raft membrane domains.
We decided therefore to analyze protein organization in the axolemma as a measure of raft integrity. Immunohistochemical analysis, confocal microscopy, and digital quantification were rigorously performed.

Our findings do not suggest a loss in neuronal membrane organization, suggesting that the increased β-amyloidogenic processing in AD is due to some mechanism other than raft disruption. This supports the findings of Simons since raft disruption would be expected to increase non-disease causing APP processing and decrease Aβ production. This opens the possibility that hyper aggregation of rafts is actually responsible for the increased β-cleavage activity that ultimately leads to the formation of amyloid plaques.

Sulfatide in Alzheimer's Disease

In the thin layer chromatography analysis of the lipid content, ST was not significantly different in the AD and non-AD brains. Our findings are in contrast to those of both Han et al., 2002 and Gottfries et al., 1996. Both of these previous studies showed a significant decrease in ST in AD.

Han and colleagues showed a 60% decrease in WM using electrospray ionization mass spectrometry, which is a more sensitive method for quantitative analysis of Sulfatide than TLC. Although TLC is a less sensitive it is unlikely that the 60% decrease observed

in the Han study would not have been detected. Gottfries et al., 1996, differentiated between early and late AD and compared them both to non-AD tissue in their study of brain lipids. They used TLC to analyze ST content in the late onset tissue and compared this to the control, revealing nearly a 40% decrease. In the present study we did not differentiate between early and late onset AD, and herein may lay the reason for the conflicting data.

Considering that we only studied white matter and Gottfries did as well, yet Han also saw a decrease in ST in GM, it is possible that the ST level decrease that is truly important in AD pathogenesis is that in GM. Since the hallmark pathologies of AD are associated with the neuron, it would very possible that a decrease in GM ST would have a direct role in AD.

Caveats

Differences in axon density, caliber, and orientation among samples were a concern due to lack of specific information on the location of harvest. This concern was essentially eliminated by standardization with axon density and qualitative analysis of axon girth. Variation in duration between time of death and time of harvesting was initially a concern since it might possibly be cause for tissue degradation due to lipidases. The white matter was largely in excellent condition suggesting that state of membrane organization revealed by the sodium channel data could be trusted. Due to the high water content in WM of live tissue and the inconsistency in post-mortem treatment of our tissue, there was a possibility that the dry weight of the tissue, and therefore total lipids, harvested varied among

samples. In order to control for this a protein assay was performed. Standardization by protein mass did not significantly change the relative ST concentrations among sample groups suggesting that variations in water content was not a significant source of error.

Literature Cited

Literature Cited

Aidley DJ (1998) The physiology of excitable cells, 4th Edition. Cambridge, UK ; New York, NY, USA: Cambridge University Press.

Armstrong R (2006) Plaques and tangles and the pathogenesis of Alzheimer's disease. Folia Neuropathol 44:1-11.

Arroyo EJ, Scherer SS (2000) On the molecular architecture of myelinated fibers. Histochem Cell Biol 113:1-18.

Baumann K, Mandelkow E, Biernat J, Piwnica-Worms H, Mandelkow E (1993) Abnormal Alzheimer-like phosphorylation of tau-protein by cyclin-dependent kinases cdk2 and cdk5. FEBS Lett 336:417-424.

Bhat MA, Rios JC, Lu Y, Garcia-Fresco GP, Ching W, St Martin M, Li J, Einheber S, Chesler M, Rosenbluth J, Salzer JL, Bellen HJ (2001) Axon-glia interactions and the domain organization of myelinated axons requires neurexin IV/Caspr/Paranodin. Neuron 30:369-383.

Boiko T, Rasband MN, Levinson SR, Caldwell JH, Mandel G, Trimmer JS, Matthews G (2001) Compact myelin dictates the differential targeting of two sodium channel isoforms in the same axon. Neuron 30:91-104.

Braak H, Braak E (1991) Neuropathological stageing of Alzheimer-related changes. Acta Neuropathol (Berl) 82:239-259.

Brown W, Moody D, Thore C, Challa V (2000) Cerebrovascular pathology in Alzheimer's disease and leukoaraiosis. Ann N Y Acad Sci 903:39-45.

Brunk UT, Terman A (2002) Lipofuscin: mechanisms of age-related accumulation and influence on cell function. Free Radic Biol Med 33:611-619.

Chen TY, Liu PH, Ruan CT, Chiu L, Kung FL (2006) The intracellular domain of amyloid precursor protein interacts with flotillin-1, a lipid raft protein. Biochem Biophys Res Commun 342:266-272.

Coetzee T, Suzuki K, Popko B (1998) New perspectives on the function of myelin galactolipids. Trends Neurosci 21:126-130.

Craner MJ, Lo AC, Black JA, Waxman SG (2003) Abnormal sodium channel distribution in optic nerve axons in a model of inflammatory demyelination. Brain 126:1552-1561.

DeArmond (1997), 3rd Edition. Baltimore: Williams & Wilkins.

Drewes G, Lichtenberg-Kraag B, Doring F, Mandelkow E, Biernat J, Goris J, Doree M, Mandelkow E (1992) Mitogen activated protein (MAP) kinase transforms tau protein into an Alzheimer-like state. EMBO J 11:2131-2138.

Dugandzija-Novakovic S, Koszowski A, Levinson S, Shrager P (1995) Clustering of Na+ channels and node of Ranvier formation in remyelinating axons. J Neurosci 15:492-503.

Dupree J (1996) Cellular Elements, Tissue Organization, Organogenesis. Boca Raton: CRC Press.

Dupree J, Girault J, Popko B (1999) Axo-glial interactions regulate the localization of axonal paranodal proteins. J Cell Biol 147:1145-1152.

Dupree J, Mason J, Marcus J, Stull M, Levinson R, Matsushima G, Popko B (2005) Oligodendrocytes assist in the maintenance of sodium channel clusters independent of the myelin sheath. Neuron Glia Biol 1:1-14.

Ehehalt R, Keller P, Haass C, Thiele C, Simons K (2003a) Amyloidogenic processing of the Alzheimer beta-amyloid precursor protein depends on lipid rafts. J Cell Biol 160:113-123.

Ehehalt R, Keller P, Haass C, Thiele C, Simons K (2003b) Amyloidogenic processing of the Alzheimer beta-amyloid precursor protein depends on lipid rafts. J Cell Biol 160:113-123.

Einheber S, Zanazzi G, Ching W, Scherer S, Milner T, Peles E, Salzer J (1997) The axonal membrane protein Caspr, a homologue of neurexin IV, is a component of the septate-like paranodal junctions that assemble during myelination. J Cell Biol 139:1495-1506.

Giese KP, Ris L, Plattner F (2005) Is there a role of the cyclin-dependent kinase 5 activator p25 in Alzheimer's disease? Neuroreport 16:1725-1730.

Gottfries C, Karlsson I, Svennerholm L (1996) Membrane components separate early-onset Alzheimer's disease from senile dementia of the Alzheimer type. Int Psychogeriatr 8:365-372.

Greenfield J, Tsai J, Gouras G, Hai B, Thinakaran G, Checler F, Sisodia S, Greengard P, Xu H (1999) Endoplasmic reticulum and trans-Golgi network generate distinct populations of Alzheimer beta-amyloid peptides. Proc Natl Acad Sci U S A 96:742-747.

Griffith LC, Lu CS, Sun XX (2003) CaMKII, an enzyme on the move: regulation of temporospatial localization. Mol Interv 3:386-403.

Han X, M Holtzman D, McKeel DJ, Kelley J, Morris J (2002) Substantial sulfatide deficiency and ceramide elevation in very early Alzheimer's disease: potential role in disease pathogenesis. J Neurochem 82:809-818.

Hof PR, Mobbs CV (2001) Functional neurobiology of aging. San Diego: Academic Press.

Honke K, Tsuda M, Hirahara Y, Ishii A, Makita A, Wada Y (1997) Molecular cloning and expression of cDNA encoding human 3'-phosphoadenylylsulfate:galactosylceramide 3'-sulfotransferase. J Biol Chem 272:4864-4868.

Honke K, Hirahara Y, Dupree J, Suzuki K, Popko B, Fukushima K, Fukushima J, Nagasawa T, Yoshida N, Wada Y, Taniguchi N (2002) Paranodal junction formation and spermatogenesis require sulfoglycolipids. Proc Natl Acad Sci U S A 99:4227-4232.

Hussain I, Powell D, Howlett DR, Tew DG, Meek TD, Chapman C, Gloger IS, Murphy KE, Southan CD, Ryan DM, Smith TS, Simmons DL, Walsh FS, Dingwall C, Christie G (1999) Identification of a novel aspartic protease (Asp 2) as beta-secretase. Mol Cell Neurosci 14:419-427.

Iqbal K, Alonso A, Gong C, Khatoon S, Singh T, Grundke-Iqbal I (1994) Mechanism of neurofibrillary degeneration in Alzheimer's disease. Mol Neurobiol 9:119-123.

Ishibashi T, Dupree J, Ikenaka K, Hirahara Y, Honke K, Peles E, Popko B, Suzuki K, Nishino H, Baba H (2002) A myelin galactolipid, sulfatide, is essential for maintenance of ion channels on myelinated axon but not essential for initial cluster formation. J Neurosci 22:6507-6514.

Ishizuka I (1997) Chemistry and functional distribution of sulfoglycolipids. Prog Lipid Res 36:245-319.

Kalvodova L, Kahya N, Schwille P, Ehehalt R, Verkade P, Drechsel D, Simons K (2005) Lipids as modulators of proteolytic activity of BACE: involvement of cholesterol, glycosphingolipids, and anionic phospholipids in vitro. J Biol Chem 280:36815-36823.

Kaplan M, Cho M, Ullian E, Isom L, Levinson S, Barres B (2001) Differential control of clustering of the sodium channels Na(v)1.2 and Na(v)1.6 at developing CNS nodes of Ranvier. Neuron 30:105-119.

Kaplan MR, Meyer-Franke A, Lambert S, Bennett V, Duncan ID, Levinson SR, Barres BA (1997) Induction of sodium channel clustering by oligodendrocytes. Nature 386:724-728.

Karas GB, Scheltens P, Rombouts SA, Visser PJ, van Schijndel RA, Fox NC, Barkhof F (2004) Global and local gray matter loss in mild cognitive impairment and Alzheimer's disease. Neuroimage 23:708-716.

Klein WL (2002) Abeta toxicity in Alzheimer's disease: globular oligomers (ADDLs) as new vaccine and drug targets. Neurochem Int 41:345-352.

Kokubo Y, Kuzuhara S (2004) Neurofibrillary tangles in ALS and Parkinsonism-dementia complex focus in Kii, Japan. Neurology 63:2399-2401.

Kourie JI (2001) Mechanisms of amyloid beta protein-induced modification in ion transport systems: implications for neurodegenerative diseases. Cell Mol Neurobiol 21:173-213.

Krafft C, Neudert L, Simat T, Salzer R (2005) Near infrared Raman spectra of human brain lipids. Spectrochim Acta A Mol Biomol Spectrosc 61:1529-1535.

Kramer E, Klein C, Koch T, Boytinck M, Trotter J (1999) Compartmentation of Fyn kinase with glycosylphosphatidylinositol-anchored molecules in oligodendrocytes facilitates kinase activation during myelination. J Biol Chem 274:29042-29049.

Lee G, Thangavel R, Sharma VM, Litersky JM, Bhaskar K, Fang SM, Do LH, Andreadis A, Van Hoesen G, Ksiezak-Reding H (2004) Phosphorylation of tau by fyn: implications for Alzheimer's disease. J Neurosci 24:2304-2312.

Mandelkow E, Drewes G, Biernat J, Gustke N, Van Lint J, Vandenheede J, Mandelkow E (1992) Glycogen synthase kinase-3 and the Alzheimer-like state of microtubule-associated protein tau. FEBS Lett 314:315-321.

Marcus J, Popko B (2002) Galactolipids are molecular determinants of myelin development and axo-glial organization. Biochim Biophys Acta 1573:406-413.

Marcus J, Honigbaum S, Shroff S, Honke K, Rosenbluth J, Dupree J (2006) Sulfatide is essential for the maintenance of CNS myelin and axon structure. Glia 53:372-381.

Markesbery W (1999) The role of oxidative stress in Alzheimer disease. Arch Neurol 56:1449-1452.

Matsuo E, Shin R, Billingsley M, Van deVoorde A, O'Connor M, Trojanowski J, Lee V (1994) Biopsy-derived adult human brain tau is phosphorylated at many of the same sites as Alzheimer's disease paired helical filament tau. Neuron 13:989-1002.

Menegoz M, Gaspar P, Le Bert M, Galvez T, Burgaya F, Palfrey C, Ezan P, Arnos F, Girault J (1997) Paranodin, a glycoprotein of neuronal paranodal membranes. Neuron 19:319-331.

Merrill AH, Jr., Schmelz EM, Dillehay DL, Spiegel S, Shayman JA, Schroeder JJ, Riley RT, Voss KA, Wang E (1997) Sphingolipids--the enigmatic lipid class: biochemistry, physiology, and pathophysiology. Toxicol Appl Pharmacol 142:208-225.

Minghetti L (2005) Role of inflammation in neurodegenerative diseases. Curr Opin Neurol 18:315-321.

Monaco EA, 3rd (2004) Recent evidence regarding a role for Cdk5 dysregulation in Alzheimer's disease. Curr Alzheimer Res 1:33-38.

Norton WT, Abe T, Poduslo SE, DeVries GH (1975) The lipid composition of isolated brain cells and axons. J Neurosci Res 1:57-75.

Patrick GN, Zukerberg L, Nikolic M, de la Monte S, Dikkes P, Tsai LH (1999) Conversion of p35 to p25 deregulates Cdk5 activity and promotes neurodegeneration. Nature 402:615-622.

Rajendran L, Simons K (2005) Lipid rafts and membrane dynamics. J Cell Sci 118:1099-1102.

Rios J, Melendez-Vasquez C, Einheber S, Lustig M, Grumet M, Hemperly J, Peles E, Salzer J (2000) Contactin-associated protein (Caspr) and contactin form a complex that is targeted to the paranodal junctions during myelination. J Neurosci 20:8354-8364.

Sato C, Yu R (1990) Heterosis for brain cerebroside synthesis in mice. Dev Neurosci 12:153-158.

Schmitt F, Cragar D, Ashford J, Reisberg B, Ferris S, Mobius H, Stoffler A (2002) Measuring cognition in advanced Alzheimer's disease for clinical trials. J Neural Transm Suppl:135-148.

Simons K, Ikonen E (1997) Functional rafts in cell membranes. Nature 387:569-572.

Simons K, Ehehalt R (2002) Cholesterol, lipid rafts, and disease. J Clin Invest 110:597-603.

Sjobeck M, Haglund M, Englund E (2006) White matter mapping in Alzheimer's disease: A neuropathological study. Neurobiol Aging 27:673-680.

Stout J, Jernigan T, Archibald S, Salmon D (1996) Association of dementia severity with cortical gray matter and abnormal white matter volumes in dementia of the Alzheimer type. Arch Neurol 53:742-749.

Suzuki A, Hoshi T, Ishibashi T, Hayashi A, Yamaguchi Y, Baba H (2004) Paranodal axoglial junction is required for the maintenance of the Nav1.6-type sodium channel in the node of Ranvier in the optic nerves but not in peripheral nerve fibers in the sulfatide-deficient mice. Glia 46:274-283.

Tait S, Gunn-Moore F, Collinson J, Huang J, Lubetzki C, Pedraza L, Sherman D, Colman D, Brophy P (2000) An oligodendrocyte cell adhesion molecule at the site of assembly of the paranodal axo-glial junction. J Cell Biol 150:657-666.

Trojanowski JQ, Lee VM (2005) Pathological tau: a loss of normal function or a gain in toxicity? Nat Neurosci 8:1136-1137.

Vetrivel KS, Thinakaran G (2006) Amyloidogenic processing of beta-amyloid precursor protein in intracellular compartments. Neurology 66:S69-73.

Vetrivel KS, Cheng H, Lin W, Sakurai T, Li T, Nukina N, Wong PC, Xu H, Thinakaran G (2004) Association of gamma-secretase with lipid rafts in post-Golgi and endosome membranes. J Biol Chem 279:44945-44954.

Vos J, Lopes-Cardozo M, Gadella B (1994) Metabolic and functional aspects of sulfogalactolipids. Biochim Biophys Acta 1211:125-149.

Zoller I, Bussow H, Gieselmann V, Eckhardt M (2005) Oligodendrocyte-specific ceramide galactosyltransferase (CGT) expression phenotypically rescues CGT-deficient mice and demonstrates that CGT activity does not limit brain galactosylceramide level. Glia 52:190-198.

VITA

Charles Britton Beasley, Jr. was born in Chapel Hill, NC on April 27, 1976. He graduated from Kinston High School in Kinston, NC and from the University of North Carolina at Chapel Hill with a B.S. in Biology. He currently resides in Richmond, Virginia.